ORIGINAL PAPER

Optimization of ANFIS controller for solar/battery sources fed UPQC using an hybrid algorithm

Koganti Srilakshmi[1] · Gummadi Srinivasa Rao[2] · Katragadda Swarnasri[3] · Sai Ram Inkollu[4] · Krishnaveni Kondreddi[5] · Praveen Kumar Balachandran[6] · Ilhami Colak[7]

Abstract

This study introduces an integrated power quality (PQ) conditioner, referred to as UPQC, that is linked with photovoltaic (PV) and battery energy systems (BSS) in order to address and solve PQ issues. It is proposed to employ the Levenberg–Marquardt (LM) backpropagation (LMBP) trained artificial neural network control (ANNC) technique for generating reference signal for converters in UPQC. This approach eliminates the need for traditional abc to dq0 to αβ conversions. Additionally, the hybrid algorithm (FFHSA) in combination of harmony search algorithm (HSA), and firefly algorithm (FFA) is also implemented for the optimal selection of adaptive neuro-fuzzy interface system (ANFIS) parameters to maintain direct current link capacitor voltage (DLCV) constant. The prime goal of the developed hybrid ANNC-FFHSA is to stabilize the DLCV with low settling time during load and solar irradiation (G), Temperature (T) changes, minimization of distortions in the source current signal to diminish total harmonic distortion (THD) in turn boosting the power factor (PF), suppression of fluctuations like disturbances, swell, sag and unbalances in the supply voltage. The suggested method is validated by four test cases with several combinations of variable irradiation (G), temperature and loads. On the other hand, to reveal the superiority of the developed method, the comparison is carried out with the genetic algorithm (GA) and Ant colony algorithm (ACA) along with instantaneous power (p–q) and Synchronous reference frame (SRF) conventional methods. The proposed approach significantly diminishes the total harmonic distortion to values of 3.61%, 3.48%, 3.48%, and 4.51%, which are notably lower compared to the values reported in the existing literature and also improves the power factor to almost unity. The design and implementation of this method were carried out using MATLAB/Simulink software.

Keywords Harmony search optimization · Firefly algorithm · Unified power quality conditioner (UPQC) · Power factor · Power quality

✉ Praveen Kumar Balachandran
praveenbala038@gmail.com

Koganti Srilakshmi
kogantisrilakshmi29@gmail.com

Gummadi Srinivasa Rao
vasu1in@vrsiddhartha.ac.in

Katragadda Swarnasri
swarnasrik@gmail.com

Sai Ram Inkollu
inkollusiaram@gmail.com

Krishnaveni Kondreddi
krishnaveni_eee@cbit.ac.in

Ilhami Colak
ilhcol@gmail.com

[1] Department of Electrical and Electronics Engineering, Sreenidhi Institute of Science & Technology, Hyderabad, Telangana 501301, India

[2] Department of Electrical and Electronic Engineering, Velagapudi Ramakrishna Siddhartha Engineering College, Kanuru, Vijayawada, Andhra Pradesh, India

[3] Department of Electrical and Electronics Engineering, R.V.R. & J.C. College of Engineering, Guntur, Andhra Pradesh, India

[4] Department of Electrical and Electronics Engineering, R. K. College of Engineering, Vijayawada, Andhra Pradesh, India

[5] Department of Electrical and Electronics Engineering, Chaitanya Bharathi Institute of Technology, Hyderabad, Telangana, India

[6] Department of Electrical and Electronics Engineering, Vardhaman College of Engineering, Hyderabad, Telangana 501218, India

[7] Department of Electrical and Electronics Engineering, Faculty of Engineering and Architectures, Nisantasi University, 34398 Istanbul, Turkey

1 Introduction

In the recent years, incorporation of distributed generation like wind, tidal, solar, etc. into the distribution network is supported in order to minimize the burden and stress on the converters and ratings. The solar integrated UPQC was implemented to resolve PQ issues efficiently. In addition a novel fuzzy-based proportional integral controller (PI-C) was designed for Maximum power tracking technique for extract maximum power and to balance DLCV [1]. Besides, the double-stage UPQC with solar PV was suggested to handle voltage and current related issues based on unit vector generation technique (UVTG) [2]. Next, the three-level UPQC with ANN-based reference signal generation was suggested to handle the PQ issues and also to eliminate complex p-q transformations [3]. However, the UPQC in association to the solar battery system with ANN-based reference signal generation was proposed to handle the PQ issues and also to eliminate complex p-q transformations [4]. Further, the fuzzy back computation was adopted for DLCV stabilization and reference signal generation to minimize the voltage and current THD [5].

The various existing algorithms for controlling the operation of SHAPF and harmonics isolation techniques, DLCV regulation, current control methods were are discussed [6]. Meanwhile, the hybrid series active power filter was implemented with ANFIS controller to suppress the THD in voltage harmonics generated by nonlinear loads [7]. The distributed generation, which combines wind and PV, was built with the goal of creating an effortless transition between the grid to the island & vice versa while preventing load changes [8]. Meanwhile, the Solar-PV powered UPQC was presented to reduced grid current THD during voltage fluctuations like sag, swell by adopting ANN, and in addition the proposed method was compared with SRF and reactive power theory methods under varying load conditions [9]. Besides, particle swarm and grey wolf algorithms was chosen to achieve the PI-C's optimal K_p, K_i values for SHAPF with a goal of controlling the power successfully and diminishing the distortions in current signal [10]. However, to keep the DLCV constant and to manage the power, the feedforward-based ANN was designed for wind system and solar PV system of UPQC [11]. A new ANN control-based reference signal generation was suggested for solar fuzzy-based MPPT battery system of UPQC to address PQ problems [12]. Future, a multilevel voltage source converter (VSC)-based UPQC was linked to the fuel cell with PV and wind system-based microgrid with an intention of handling PQ issues efficiently [13]. Meanwhile, the comprehensive analysis was done on several kinds of phased synchronize techniques which are suitable for the control and operation of SHAPF [14]. However,

the GW-O-based PI-C was suggested for various loading conditions of UPQC with a view of minimizing THD [15].

A new method was proposed to UPQC for the quick action in fault reorganization with good accuracy in addition stabilizing DLCV oscillations [16]. The artificial neuro-based fuzzy hybrid control scheme was designed to UPQC for addressing grid voltage problems like swell, THD, sag etc. and load current THD efficiently [17]. The hybridization of both Improvedbat and Mothflame metaheuristic optimization methods for selection of gain parameters of PIC was suggested to address the PQ issues [18]. The fuzzy logic controller (FLC) was suggested for SEAF for the local distribution system to eliminate the voltage fluctuations and current THD effectively [19]. A Soccer match optimization for optimal design of ANNC was suggested to PV and BSS integrated UPQC to solve PQ issues in distribution system [20]. An adaptive hysteresis band with fuzzy logic controller (FL-C) was designed to the PV associated 9-level VSC-based UPQC with an aim of obtaining fluctuations free voltage waveforms [21]. A Soccer-league optimization was proposed for the optimal selection of gain parameters of PIC for UPQC to handle both voltage fluctuations and current distortions successfully [22]. The ANN-based reference gate pulse generation method was developed for five-level UPQC to handle current and voltage distortions successfully [23].

The UPQC controller achieved phase synchronization through the utilization of a STF combined with the UVGT. The successful execution of the Self-Tuning Filter (STF) in UPQC eliminated the requirement for a PLL, and the STF with UVGT method was employed to generate synchronization phases for both filters of UPQC [24]. Besides, a harmonic compensation method tailored for hybridized AC-DC converter operating for low switching frequency was introduced. The proposed approach was explored, covering the discussions on the approach, modeling schemes, stability studies [25]. Meanwhile, the development of a SAPF was aimed at regulating grid-integrated PV systems to mitigate harmonic distortions. The PV-integrated SAPF effectively supplies active and reactive power to the grid to reduce harmonic components. Furthermore, adaptive techniques such as ANN like ANFIS, Widrow–Hoff Adaptive Linear Neuron, and Modified Widrow–Hoff Adaptive Linear Neuron were utilized to create the reference current for the Inverter [26].

An enhanced photovoltaic system was combined with a hybrid filter to enhance the PQ in distribution network. The shunt filter was developed, incorporating photo-voltaic, utilizing an advanced signal processing technique known as the dual-tree complex wavelet transform to extract frequency-related information from the voltage and current signals

caused by PQ disturbances [27]. Moreover, an economical Hybrid Shunt Active Power Filter was introduced to address the issue of THD. Furthermore, a unique inference method was employed to calculate the per-unit fundamental component of the reference current in-phase. In addition, a new Fuzzy-PID Controller was utilized to maximize the reference current value. The optimization of all controller parameters was carried out using an Enhanced Football Game Optimization method [28]. Furthermore, in order to mitigate disadvantages, a hybrid SHAPF was devised. The calculation of the reference current involved the utilization of the dual-tree complex wavelet transform (DT-CWT), while the optimization of the parameters for the HSAPF system was achieved through the application of conventional proportional-integral (CPI) control, as well as type-1 and type-2 fuzzy logic controllers (T1FLC and T2FLC). This approach was adopted to enhance the system's capability to compensate for harmonics and improve power factor [29].

Majority of the literature papers using evolutionary algorithms attempted only to tune parameters of the conventional PIC. It also illustrates that the traditional techniques for UPQC currently in use involve complex Clarke's and Park's changes. This research proposes an innovative artificial intelligence (AI) scheme, in conjunction with PV and BSS, incorporating an ANN approach, and it optimizes the ANFIS controller parameters of UPQC using FFHSA.

The prime contribution of this work is as follows:

- An ANNC scheme trained with LMBP is recommended to produce required reference signals for VSCs, thereby avoiding the need for traditional abc to dq0 to αβ conversions, such as p-q and SRF methods.
- FFHSA is suggested for optimal selection of fuzzy MSF parameters and weights of ANFIS controller for DC Link.
- The prime goal of the developed ANNC-FFHSA is to suppress the distortions in source current signal and in turn enhancing the PF, handling the grid voltage related PQ issues like (sag, swell, disturbance, unbalances etc.)
- The PV with BSS is associated to the UPQC's DC link to meet the load demand, quick response in maintaining constant DLCV during variable load and irradiation to minimize the stress and rating of the VSC's.
- Additionally, the suggested ANNC-FFHSA for PV and energy BSS integrated UPQC (UPVBSS) is validated on four test studies for several combinations of supply voltages, G, temperature, loading conditions to reveal the overall performance w.r.t the current THD, PF through the waveforms.
- However, to reveal the viability of the suggested method THD, and DLCV settling time is compared with GA and PS–O algorithms in addition to p–q and SRF methods.

The manuscript is structured as follows: Sect. 1 provides an introduction, Sect. 2 covers the design of proposed UPVBSS, Sect. 3 elaborates on the control scheme, Sect. 4 discusses the obtained results, and, lastly, Sect. 5 serves as the conclusion of the paper.

2 Design of proposed system

The developed UPQC arrangement is depicted in Fig. 1. In this setup, solar PV is linked to the DC link of the UPQC via a boost converter, while the BSS is connected through a buck-boost converter. In this context, "V_{abc}" denotes the supply side voltages, "V_{s_abc}" represents the phase voltages at the source bus, and "V_l" and "i_l" refer to current and voltage at the load terminals. "R_s" designates the grid side resistance, and "L_s" signifies the source inductance. The UPQC combines both series and shunt VSCs. The primary purpose of the SAPF is to address voltage-related issues on the grid side by supplying appropriate compensation voltage "V_{se}" through an injecting transformer. The RL filter consists of a resistor "R_{se}" and an inductor "L_{se}." The SHAPF is connected through resistance, interfacing inductance "L_{sh}," and capacitance "C_{sh}" to the grid. The SHAPF's objective is to reduce harmonics in the current signal and maintain DLCV at a constant level with minimal settling time by injecting the necessary current "i_{sh}".

2.1 External support for direct current-link

The incorporation of solar/battery to the UPQC's DClink reduces the requirement of large ratings and burden on converters with lower demand from the utility. Here, Boost Converter (B–C) is used to boost the output of solar system and the charge and discharge of battery attached to the DC's link is handled with Buck-Boost converters (B–B–C) to regulate the DLCV during variation in loads. As the modeling of PV and Battery systems are already available in the literature [5], the control circuit of PV and battery is explained. The equation for DClink power demand (P_{dc}) of the suggested technique is given in Eq. (1).

$$P_{PV} + P_{BSS} - P_{dc} = 0 \tag{1}$$

2.1.1 Solar power generating (SPG)

Solar system transfers the sun's irradiation into electric power. The quantity of PV cells connected in series and in parallel plays a pivotal role in determining the necessary solar generation capacity. In this work PV model is taken from simulink library. As the modeling of PV is available in the
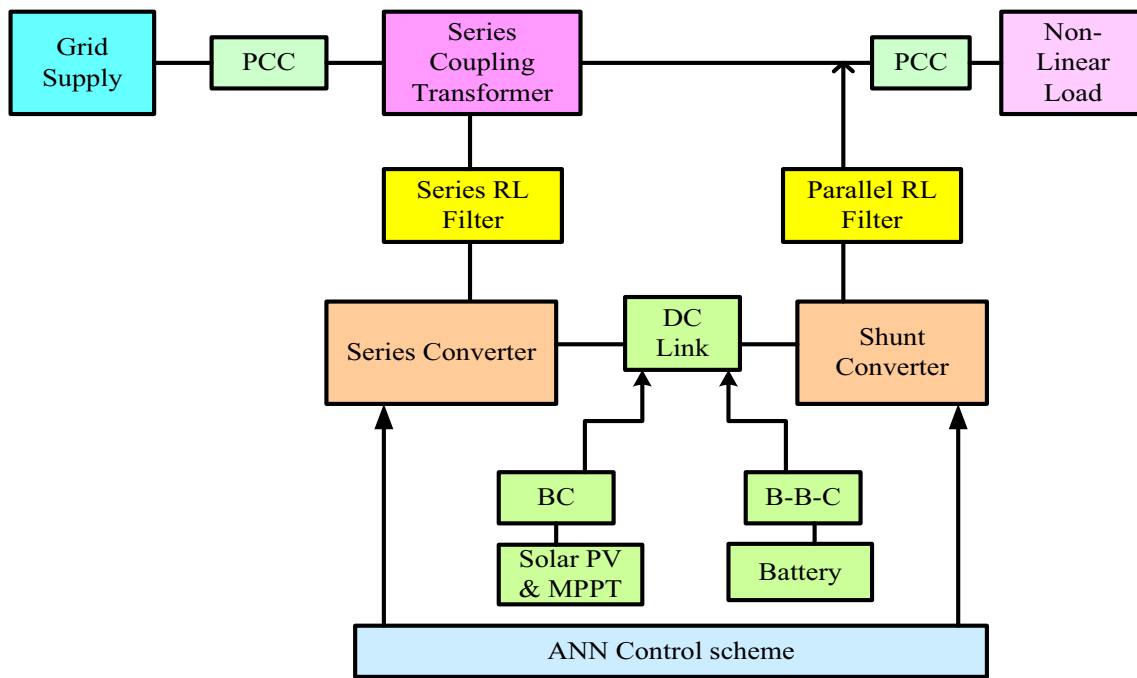
Fig. 1 Block diagram of proposed UPQC

literature, this work mainly focuses on the optimal design of controller. The power of PV system (P_{PV}) is given by Eq. (2)

$$P_{PV} = V_{PV} \times i_{PV} \qquad (2)$$

where V_{PV}, i_{PV} implies the output voltage and current of photovoltaic panel. In this study, the Maximum Power Point Tracking (MPPT) employs the Perturb and Observe (P & O) a widely used method for maximizing the efficiency of solar photovoltaic systems or other renewable energy sources by continuously adjusting the operating point of the power converter to track the maximum power point (MPP). This technique involves perturbing (slightly changing) the operating conditions and observing the resulting change in power output. Here, it is used to regulate the duty cycle (ΔD) of the boost converter, as illustrated in Fig. 2. The adjustment in duty cycle is determined by assessing alterations in power (ΔP) and voltage (ΔV). When power increases, the algorithm raises the voltage, and conversely, when power decreases, it reduces the voltage.

2.1.2 BSS

The BSS supports in stabilizing the DLCV. The state-of-charge-of-battery (SOCB) is expressed in Eq. (3).

$$SOCB = 100(1 + \int i_{BSS} \, dt \, Q) \qquad (3)$$

The SPG output will decide the operational condition of a BSS, whether it should discharge or charge, while fulfilling to the constraints specified in Eq. (4).

$$SOCB_{min} \leq SOCB \leq SOCB_{max} \qquad (4)$$

By minimizing the DLCV error $V_{dc,err}$ by a PI-C, the i^{ref}_{dc} is calculated. By using PI-C, the battery error reference current $i_{BS,err}{}^*$ is computed. Where, $i_{BS,err}$ represents the discrepancy between the battery reference current i^{ref}_{BS} received from LPF and the i^{ref}_{dc} obtained from it. The graphical representation of energy management at DC link is illustrated in Fig. 3. If the solar power produced is greater than the required DC link power, the excess solar power is used to charge battery if SOCB is less than its higher limit. Similarly, if solar power produced is lower than the required DC link power, the remaining power is supplied by the battery if the SOCB is greater that its lower limit. The complete control circuit of PV and battery systems with the proposed UPQC system is exhibited in Fig. 4.

2.2 Capacitor value at DC link

The value of C_{dc} can be calculated [5] by Eq. (5).

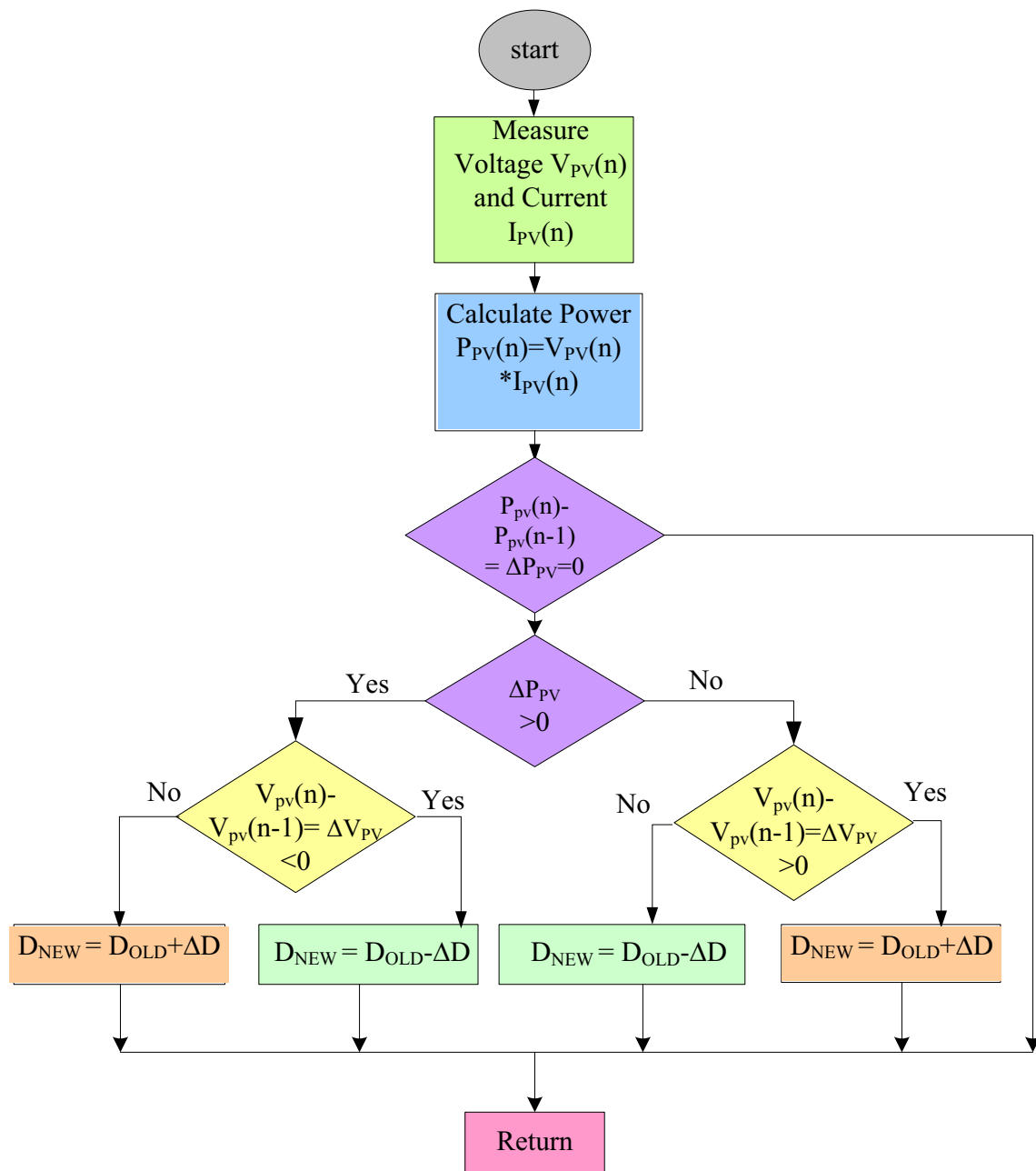$$C_{dc} = \frac{\pi * i_{sh}}{\sqrt{3}\omega V_{cr,pp}} \qquad (5)$$

Fig. 2 P&O MPPT algorithm flow chart

The V_{dc}^{ref} is selected within the allowable ratings of the proposed system. The selection of C_{dc} depends on peak to peak voltage ripple ($V_{cr,pp}$) and shunt compensating current.

2.3 Inductor for shunt and series VSC with isolation transformer

With the support of an inductor (L_{sh}), the shunt VSC is connected to the network. Equation (6) provides the switching frequency, ripple current, and DLCV.

$$L_{sh,min} = \frac{\sqrt{3}\, m\, V_{dc}}{12\, a_f\, f_{sh}\, I_{cr,pp}} \tag{6}$$

Assuming the modulation depth (m) as 1, over loading factor (a_f) is 1.5, and switching frequency (f_{sh}) is 10 kHz [24], the value of L_{sh} depends on peak to peak ripples ($I_{cr,pp}$). The connection of the series VSC to the grid is facilitated by a 3-phase series injection transformer, and its design parameters
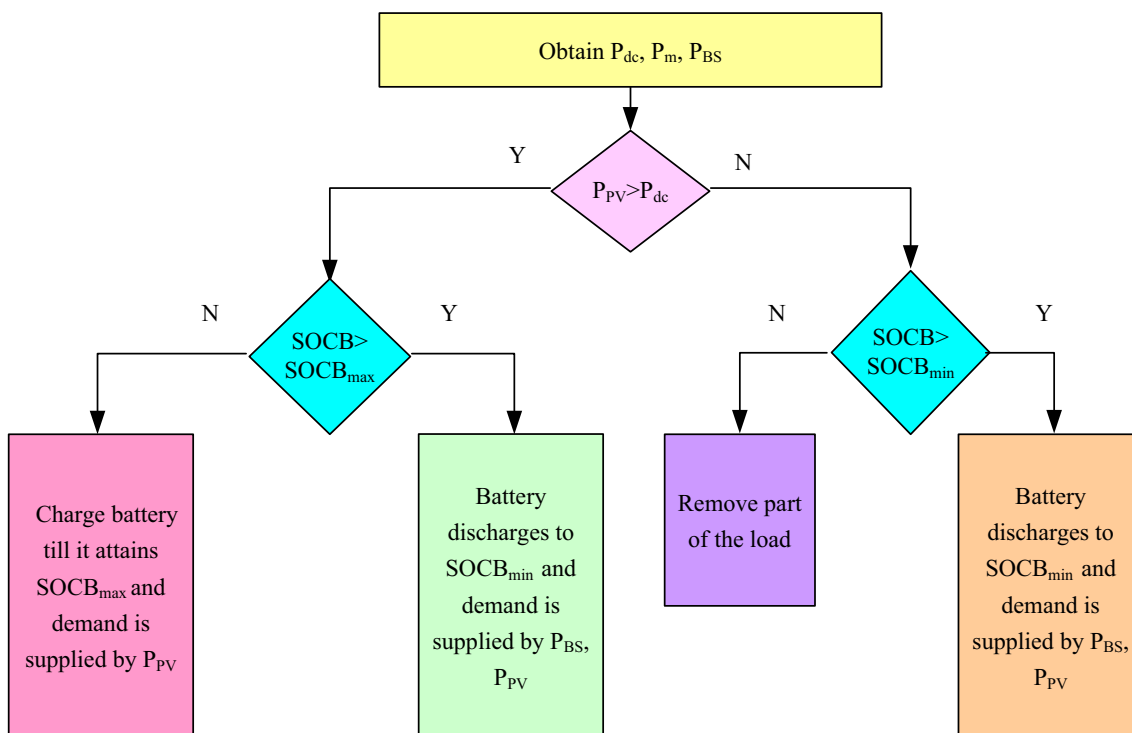
Fig. 3 Power Distribution at DC link

are defined in Eqs. (7) and (8).

$$K_{\text{se}} = \frac{V_{L-L}}{\sqrt{3}\ V_{\text{se}}} \tag{7}$$

$$L_{\text{se,min}} = \frac{\sqrt{3}\ m\ V_{\text{dc}}\ K_{se}}{12\ a_f\ f_{\text{se}}\ I_{\text{cr,pp}}} \tag{8}$$

Assuming that the switching frequency (f_{se}) is 10 kHz [24], the series inductance depends on ripple current.

3 Proposed ANN scheme

Generally, VLDC varies during the dynamic load variation. However, a quick return to the initial value is required to bring the network back to normal state of DLCV. Here, the recommended ANNC is used together with PWM hysteresis-current-control for shunt VSC and gate firing pulses for VSC.

3.1 Shunt filter

The primary objective of SHAPF is to mitigate distortions in the current signal and maintain DLCV stable in the presence of faults and varying load situation by introducing compensatory currents.

3.1.1 Proposed FFHSA for optimal design of ANFIS for DLCV balancing

The ANFIS is suggested to maintain constant DLCV. The suggested ANFIS is an intelligent hybrid controller with the combination of ANN-C and FL-C features. However, for maintaining DLCV constant, the chosen reference DLCV is compared with respect to the obtained DLCV; and its output Error (E), change in Error (CE) is considered as inputs. The inputs fed to the ANNC are initially trained according to the triangular membership function (MSF) to produce the best as shown in Fig. 5. ANFIS mainly consists of five layers, the 1st layer (Fuzzification) the outputs of this layer are fuzzy MSF given by Eq. 9

$$\begin{aligned} \mu_{\text{A}i}(x),\ i &= 1,\ 2. \\ \mu_{\text{B}j}(y),\ j &= 1,\ 2. \end{aligned} \tag{9}$$

where, $\mu_{Ai}\mu_{Bj}$ are the MSF outputs obtained from the 1st layer.

In this work, triangular MSF is selected due to its simplicity in defining and understanding. It is defined by three parameters: the lower bound (a), the peak or center value (b), and the upper bound (c). This simplicity makes them easy to work with in both theory and practical applications. Moreover, calculating the membership value for a given input is computationally efficient for triangular MSF compared to
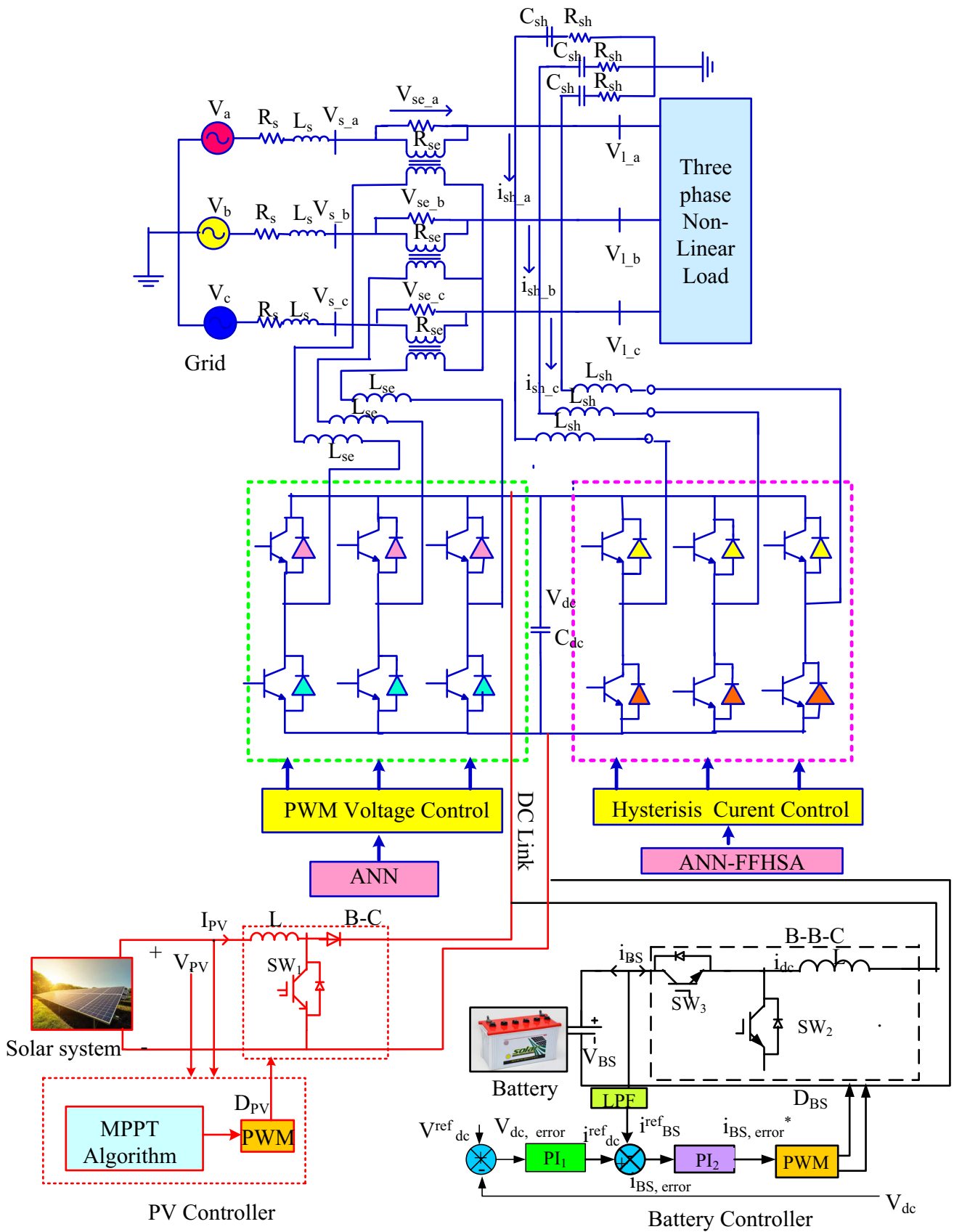
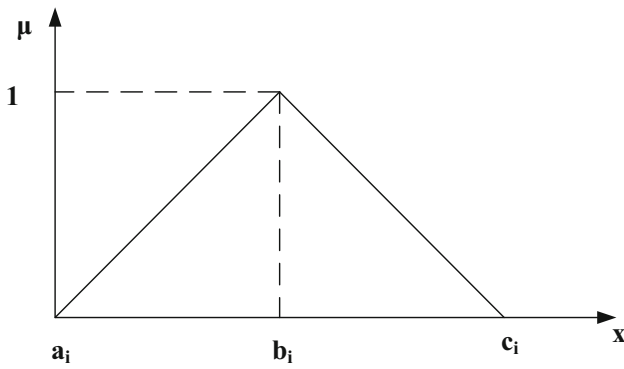**Fig. 4** Controller of proposed system

Fig. 5 Triangular MSF

other types of MSF. The mathematical representation of triangular MSF is given by Eq. 10

$$\mu_{\text{Ai}}(x) = \max(\min(\frac{x - a_i}{b_i - a_i}, \frac{c_i - x}{c_i - b_i}), 0) \tag{10}$$

where the range (universe of discourse) of x is $x_{\max} - x_{\min}$ (upper and lower bonds) and b_i is the point of maximum support of the fuzzy set i. The input and output categories include Negative-Big (NTB), Negative-Medium (NTM), Zero (ZOE), Positive-Small (PTS), Positive-Big (PTB), Positive-Medium (PTM), and Negative-Small (NTS). Figure 6 illustrates the inputs and outputs of the MSF, while Table 1 displays the fuzzy-rule base.

However, in the 2nd layer (weighting of fuzzy rules) the AND operator is applied, and calculates the firing strength w_i by adopting MSF computed in 1st layer whose output is calculated by Eq. (11).

$$w_k = \mu_{\text{Ai}}(x) * \mu_{\text{Bj}}(y)i, \ j = 1, 2. \tag{11}$$

The normalization of values takes places in the 3rd layer received from the previous layer. Each node reaches normalization by evaluating the ratio of the kth rule's firing strength (truth values) to the summation of all rule's firing strength is given Eq. (12).

$$\overline{w_k} = \frac{w_k}{w_1 + w_2} k = 1, 2. \tag{12}$$

The self-adaptive ability of the ANN-C is carried out by applying the inference parameters (p_k, q_k, r_k) in the 4th layer (defuzzification) output is given by Eq. (13).

$$\overline{w_i} f_i = \overline{w_i}(p_k u + q_k v + r_k) \tag{13}$$

Lastly, at the 5th layer inputs are get added up to produce the desired total ANFIS output by Eq. (14).

$$f = \sum_i \overline{w_i} f_i \tag{14}$$

Figure 7 shows the block diagram of the proposed ANFIS. The task is to reduce learning errors in order to improve the overall performance of the ANFIS controller by optimizing a_i, b_i and c_i of MSF parameters and the neuron weights using FF and HSA combined hybrid algorithm. The problem is formulated to minimize the objective (Ω) which is represented as MSE by evaluating the fitness or brightness function F given by Eq. 15

$$\text{Maximize} \ \ F = \frac{1}{1 + \Omega}$$

$$\Omega = \frac{1}{n} \sum_{p=1}^{m} (O_p - \overline{O}_p)^2 \tag{15}$$

Here, o is the output obtained, $\overline{o}$ is the desired, and m is the number of instance. The proposed hybrid algorithm (FFHSA) is discussed in detail.

3.1.2 Firefly algorithm (FFA)

The FFA is inspired by the flashing behavior of the set of the fireflies. Firstly, a set of fire flies are arbitrarily generated in the space. Here, every fire fly resembles the required solution, which relies totally on the selected parameters for control. Here, every firefly (y) is the control variables whose bonds are given as

$$y^k(\min) \leq y^k \leq y^k(\max); \ k = 1, 2...\text{nd} \tag{16}$$

where nd = Total variables.

This algorithm uses bioluminescent communication for the movement among the fireflies. Every firefly is mesmerized towards the brightness of another fire-fly and attempts to shift towards it. The brightness function (F) of firefly gives the suitable value of the chosen problem. In the iterative process FFA calculates F and alters their positions accordingly. The attractiveness β_{ij} between the ith, j^{th} firefly is represented by Eq. (17)

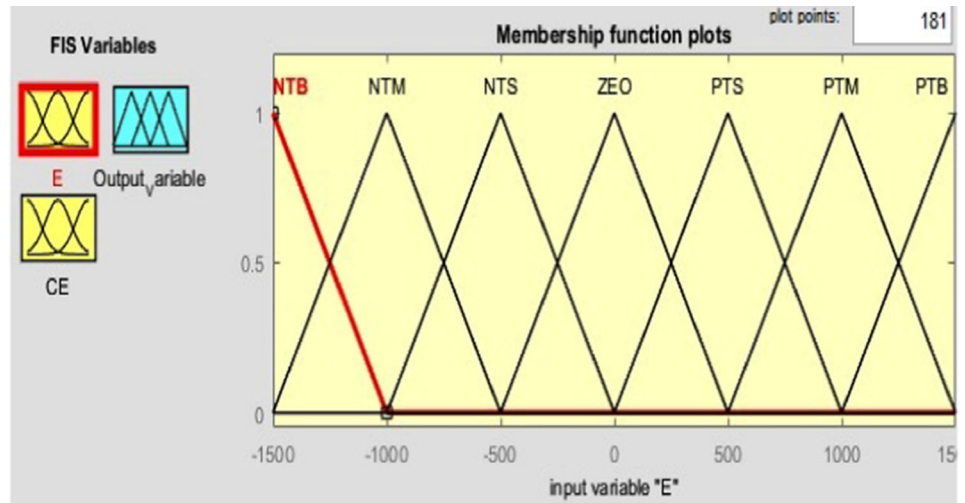$$\beta_{ij} = \beta_0 \exp(-\gamma r_{ij}^2) \tag{17}$$

where r_{ij} represents the Cartesian distance between i^{th}, j^{th} firefly and is computed by Eq. (18)

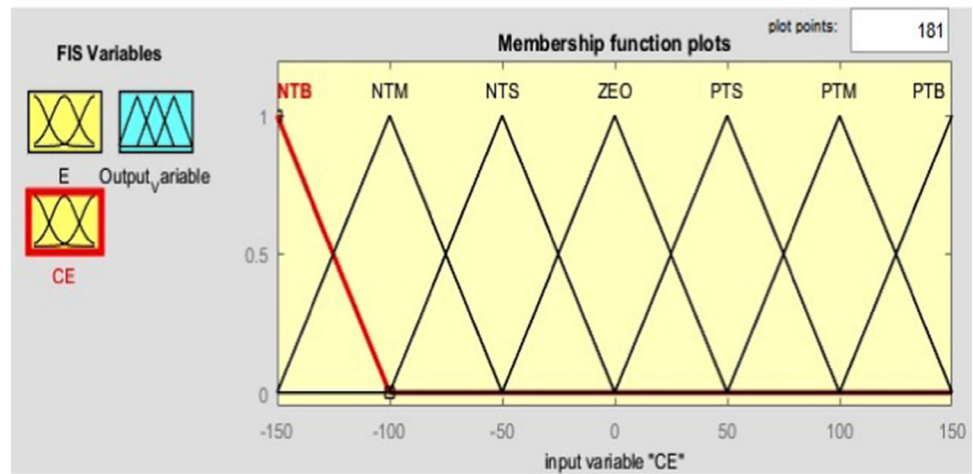$$r_{ij} = \| y_i - y_j \| = \sqrt{\sum_{k=1}^{\text{nd}} (y_i^k - y_j^k)^2} \tag{18}$$

In team, i^{th} firefly shifts towards the jth firefly and modifies its location, if BF_j is larger than BF_i at t^{th} moment by Eq. (19)

Fig. 6 Fuzzy MF for E, CE

(a) MF for E

(b) MF for CE

Table 1 Fuzzy rule-base

E	CE						
	PTB	PTM	PTS	ZEO	NTS	NTM	NTB
NTB	ZEO	NTS	NTM	NTB	NTB	NTB	NTB
NTM	PTS	ZEO	NTS	NTM	NTB	NTB	NTB
NTS	PTM	PTS	ZEO	NTS	NTM	NTB	NTB
ZEO	PTB	PTM	PTS	ZEO	NTS	NTM	NTB
PTS	PTB	PTB	PTM	PTS	ZEO	NTS	NTM
PTM	PTB	PTB	PTB	PTM	PTS	ZEO	NTS
PTB	PTB	PTB	PTB	PTB	PTM	PTS	ZEO

Fig. 7 Structure of ANFIS
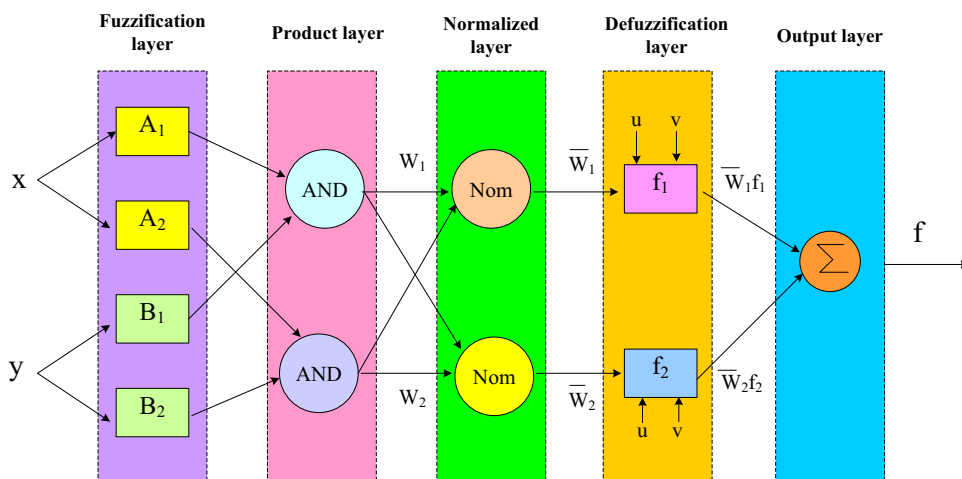
Table 2 Selected parameters for algorithms

Algorithm	Parameter	Chosen Value
FF	nf	30
	β_0	0.97
	γ	0.92
	α	0.5
	T^{max}	150
HSA	HMS	42
	HMAR	0.93
	PTR	0.09
	BW	0.13
	T^{max}	150
GA	Population count	50
	T^{max}	150
	Alpha	0.85
	Mutation	0.1
ACA	Initial pheromone (τ)	1e − 06
	Pheromone constant	1
	Global pheromone decay rate	0.9
	Local pheromone decay rate	0.5
	T^{max}	150

Table 3 BSS and PV Ratings

Device	Factor	Value
PV panel model selected (SPR-30JE-WHT-U)	Output	305.226 W
	Open-circuit-voltage	64.2 V
	Shortcircuit current	5.96A
	Voltage/ current at maximum power point	54.60 V /5.58A
	No of parallel strings, series connected modules per string	66, 5
Li-ion battery	Rated-Capacity of battery	450.0Ah
	Maximum capacity	550.0Ah
	Nominal Voltage	650 V
	maximum voltage	757 V

problem constraints. The selected parameters of the algorithms are listed in Table 2. A harmony memory (HM) comprising a number of candidate solutions, each representing a harmony, is defined in the problem space as given in Eq. 20.

$$y_i(t) = y_i(t-1) + \beta_{ij}(y_j(t-1) - y_i(t-1)) + \alpha(\text{rand} - 0.5) \tag{19}$$

$$HM = \begin{bmatrix} harm_1^1 & harm_2^1 & \cdots & harm_N^1 \\ harm_1^2 & harm_2^2 & \cdots & harm_N^2 \\ harm_1^3 & harm_2^3 & \cdots & harm_N^3 \\ \vdots & \vdots & & \vdots \\ harm_1^{HMS} & harm_2^{HMS} & \cdots & harm_N^{HMS} \end{bmatrix}$$

$$harm_i \rightarrow [harm_{i\,1}, \ harm_{i\,2}, \ \ldots, \ldots, \ldots, \ldots, harm_{i\,m}] \tag{20}$$

3.1.3 Harmony search algorithm (HSA)

It is inspired from the musicians' improvisation technique of music, is a metaheuristic iterative optimization technique and explores the problem space for optimal solution that maximizes the chosen fitness function (F) while fulfilling the

The optimal design of MSF for the FLC is selected as optimization problem with a aim of reducing the error by optimally choosing fuzzy membership parameters a_i, b_i

and c_i. The quality of each harmony is assessed by a harmony fitness function (F), formed from the objective as the chosen problem as Eq. 11. An improvised harmony $harm\prime = (harm_1\prime,\ harm_2\prime,\ L\ ,harm_N\prime)$ is generated by comparing a random number with HM adjusting rate (HMAR) value as explained in Eq. (21).

help it converge to global optima efficiently. This approach allows for parallel exploration of the search space, increasing the chances of finding the global optimum. It is less prone to getting stuck in local optima, and it often finds high-

$$
\begin{aligned}
&\text{if } (\text{rand }(\ ) < \text{HMAR}) \\
&\qquad harm_i' \leftarrow harm_i' = (harm_i^1,\ harm_i^2,\ \cdots,\ harm_i^{HMS}) \\
&\text{else} \\
&\qquad harm_i' \leftarrow harm_i' \in \{harm_i(\min) \leftrightarrow harm_i(\max)\} \\
&\text{end}
\end{aligned}
\tag{21}
$$

Where, rand () is a random number (0 ~ 1). The pitch of each variable in the improvised harmony is adjusted based on the pitch tuning rate (PTR) by Eq. 22.

quality solutions even in complex and non-convex search. Similarly, the HSA can be scaled for large-scale optimization problems by adjusting parameters and population sizes. This scalability allows it to tackle problems of varying com-

$$
\begin{aligned}
&\text{if } (\text{rand }(\ ) < \text{PTR}) \\
&\qquad harm_i' \leftarrow harm_i' \pm rand(\ ) \times BW \\
&\text{else} \\
&\qquad harm_i' \leftarrow harm_i' \\
&\text{end}
\end{aligned}
\tag{22}
$$

Where, BW denotes bandwidth. If the improvised harmony vector $harm\prime$ is superior than the worst harmony in the HM, then the worst one is replaced by the new harmony $harm\prime$. The generation of new Harmony is repeated till convergence. Based on the F value, each firefly updates position, HMAR, PTR in HSA improves the convergence process to represent the global optima solution. The process is carried out until it reaches maximum iterations ($T^{\max}$). Table 3 lists the parameters that were selected for the optimizations that were suggested and compared.

The FFA is well-suited for solving global optimization problems, where the goal is to find the best solution in a search space. Its exploration and exploitation mechanisms

plexity. Moreover, it is problem-independent it does not rely on prior knowledge of the optimization problem's mathematical structure. This makes it suitable for a wide range of real-world applications. Actually, large-scale optimization is the problem with the FFA. In a similar manner, the HSA algorithm should require improvement in terms of convergence speed. Therefore, combining the two methods is planned in order to achieve improved convergence and outcomes. In this work, the hybrid FFHSA adapts both the properties of FFA and HAS to obtain the best optimal solution. The pseudocode of the proposed hybrid algorithm is as follows:

Begin

Step 1. *Read the problem data*

Select the parameters: Set t=1; T^{max}, define γ; set α, β_0 at r=0; set HMAR, PTR, BW, HMS,

set the number of fireflies.

Step 2. *Evaluate the Brightness function F.*

Step 3. *While $t < T^{max}$*

      Sort the fireflies by brightness;

      for i=1 : assign value for i^{th} firefly (all fireflies) do

            Run simulink obtain THD using Eq. 15

     for j=1 : assign value for j^{th} firefly (all fireflies) do

            Run simulink obtain THD using Eq. 15

        if ($F_j < F_i$) then

        By computing Eq. 18, 17 move firefly j towards i by Eq. 19;

       else

            for k=1 : (all harmonies) do

                if (rand ( ) < HMAR) then

                    Apply Eq. 21

                    if (rand ( ) < PTR) then

                     Apply Eq. 22

                  end if

              end for k

        end if

        Update attractiveness;

        Update brightness;

      end for j

     end for i

     Evaluate the brightness F.

     Rank the fire flies largest brightness firefly is the required optimal solution;

     t=t+1;

Step 4. *end*

while End.

3.2 ANN control scheme for reference current signal generation

Figure 6 depicts the suggested ANN controller for the shunt filter. An input layer (IPL), output layer (OPL), and hidden layer (HIL) are present in the ANNC configuration. The IPL's goal is to gather provided data and transfer it to the HIL. It is then multiplied by the weights on the linked links that connect the IPL and HIL. In this case, mathematical computations are performed with a chosen bias on HIL. Finally, the outcomes are resolved in OPL. To get the intended result, the link's weights are adjusted during training by analysing the inaccuracy.

The Levenberg–Marquardt (LM) algorithm is a widely used optimization technique for training ANN. The LM algorithm is used to minimize the cost function by adjusting the weights and biases of the neural network. The LM algorithm relies on computing gradients, and back propagation (LMBP) is used to calculate the gradients of the cost function with respect to the network parameters (weights and biases). This involves computing the gradients layer by layer, starting from the output layer and propagating them backward through the network. During the each iteration of the LM algorithm, the network's weights and biases are updated based on the calculated gradients. The updates are determined by the LM algorithm's rules, which depend on the curvature and error in the cost function. Therefore, LMBP technique is adopted in this work to obtain faster convergence.

As seen in Fig. 8, the reference currents ($i^{\text{ref}}_{\text{sh\_a}}$, $i^{\text{ref}}_{\text{sh\_b}}$, $i^{\text{ref}}_{\text{sh\_c}}$) are regarded as target data, whereas the load currents ($i_{\text{l\_a}}$, $i_{\text{l\_b}}$, $i_{\text{l\_c}}$) and DC loss component (Δi_{dc}) acquired from FFHSA are considered as input. Additionally, Fig. 9 depicts the structure of the suggested BP for the generation of the reference current signal in the HIL using 200 neurons. It is believed that a hysteresis regulator with ± 0.25A and ± 0.5A band can generate the necessary gating signals for the shunt VSC.

3.3 Series filter

The primary contribution of SAPF is to provide appropriate compensating voltages to mitigate grid voltage fluctuations and maintain a stable voltage supply to the load. In Fig. 10, the proposed control scheme for the series VSC is depicted. The reference voltage signals ($V^{\text{ref}}_{\text{se\_a}}$, $V^{\text{ref}}_{\text{se\_b}}$, $V^{\text{ref}}_{\text{se\_c}}$) are generated using the supply voltage signals ($V_{\text{s\_a}}$, $V_{\text{s\_b}}$, and $V_{\text{s\_c}}$) as input data, while the reference voltage is considered as the target data for the ANNs. Figure 11 illustrates the ANN's structure, consisting of 200 neurons in a HIL. The gating pulses for the series VSC are produced through PWM.

4 Results with discussions

The UPVBSS with ANNC was designed using MATLAB 2016a. In Table 3, you can find the specifications for the solar system and BSS. Additionally, Table 4 displays the parameters for the system and UPQC. To demonstrate the functionality of the developed ANNC-FFHSA, four test cases were chosen, each involving various permutations of rectifier-based nonlinear loads, balanced or unbalanced source voltages, and different circumstances such as voltage swell, disturbance, and voltage sag, with varying irradiation (G) and a temperature of 25 °C, as outlined in Table 5. Specifically, for the first three studies, a balanced phase supply (V_S) was selected, while an unequal phase supply was used for case 4. The first case examined balanced voltage sag, while cases 2 and 3 focused on sag and disturbance issues. The minimization of THD, improvement in PF and maintaining constant DLCV were considered as prime motive in this work. To show the working of the proposed ANN-based FFHSA, the results are compared with GA and ACA methods. The convergence plot of MSE for proposed FFHSA in comparison with GA and ACA for case1 is given in Fig. 12. The PF is extracted from the obtained THD by Eq. 23.

$$\text{PF} = \cos\theta * \frac{1}{\sqrt{1 + \text{THD}^2}} \tag{23}$$

The magnitude of voltage during sag/ swell ($V_{\text{sag/swell}}$) is evaluated by Eq. (24)

$$V_{\text{sag/swell}} = \frac{V_l - V_S}{V_l} = \frac{V_{\text{se}}}{V_l} \tag{24}$$

The compensated voltage supplied by series converter is in Eq. (25)

$$V_{\text{se}} = V_l - V_S \tag{25}$$

The compensated current supplied by series converter is in by Eq. (26)

$$i_{\text{sh}} = i_i - i_S \tag{26}$$

For Case 1, balanced V_S is chosen, and it is used to assess the performance of SAPF. In this scenario, 30% voltage sag was intentionally introduced into the V_S from 0.25 s to 0.35 s, as depicted in Fig. 13a. The ANNC recognizes the dip, in the voltage effectively and supplies the required compensating voltage to maintain terminal voltage constant. To investigate the performance of SHAPF of proposed ANNC-FFHSA, load 1 and load 4 were considered. The load terminal current waveform is identified to be polluted with harmonics, nonsinusoidal and balanced as exhibited in Fig. 13b. The
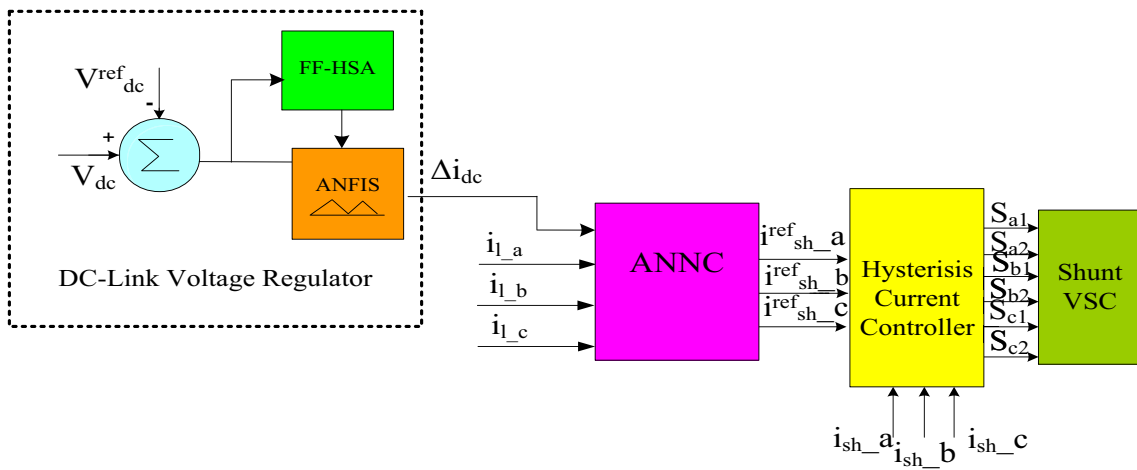
Fig. 8 Shunt VSC controller
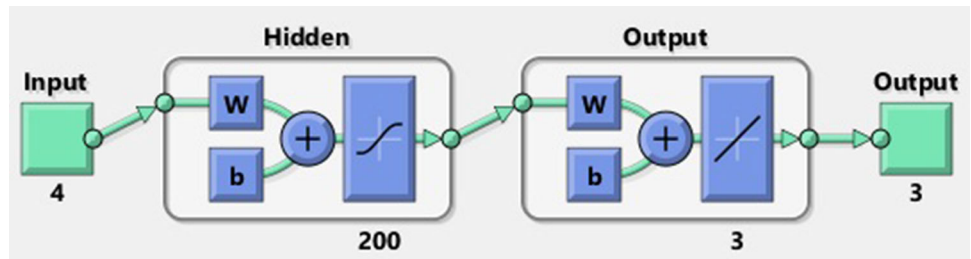
Fig. 9 structure of ANNC for reference current generation
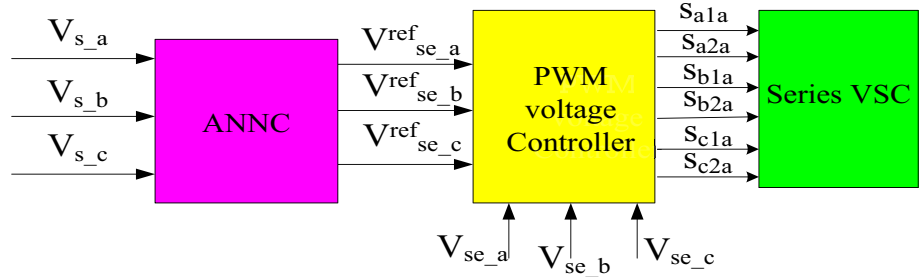

Fig. 10 Series-VSC controller
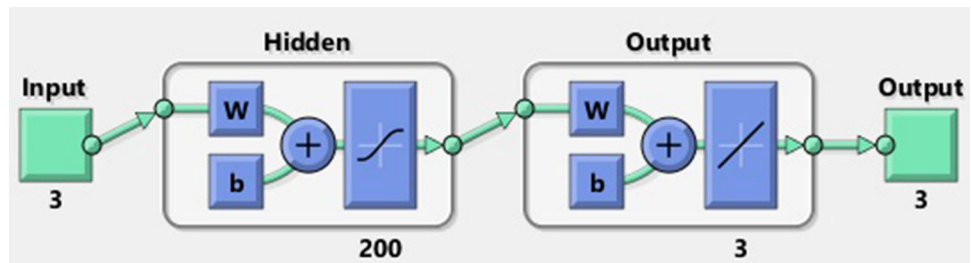

Fig.11 Series ANNC structure

Table 4 Gris system's & Device specifications

Supply	f: 50Hertz; L_s: 0.15 milliHenery; R_s: 0.1Ω; V_s: 415Volts
DClink	C_{dc}: 9400 microfarad; $V_{dc}^{ref} = 700$Volts
Loads	Bridged rectifier 3phase balanced load: L = 1mH, R = 10Ω
	Un-balanced RL branch 3 phase load: R1 = 10 Ω, R2 = 20, R3 = 15 Ω, L1 = 1.5 mH, L2 = 3.5 mH, L3 = 2.5mH
	Un-balanced 3 Φ R type load: R1 = 50 Ω, R2 = 10, R3 = 30 Ω
	Balanced nonlinear Load: P = 500 W, Q = 9000 Kvar

Table 5 Case studies

Circumstance	Case study 1	Case study 2	Case study 3	Case study 4
Balanced V_S	✓	✓	✓	
Unbalanced V_S				✓
V_{Sag}	✓			
V_{Swell}		✓		
Voltage distortion			✓	
Irradiation of 1000 w/m^2	✓		✓	
Variable Irradiance		✓		✓
Solar Temperature of 25^{0}c	✓	✓		
Solar Temperature of 24 °C			✓	✓
Load variation		✓		✓
Load 1	✓		✓	✓
Load 2		✓		✓
Load 3		✓	✓	✓
Load 4	✓			
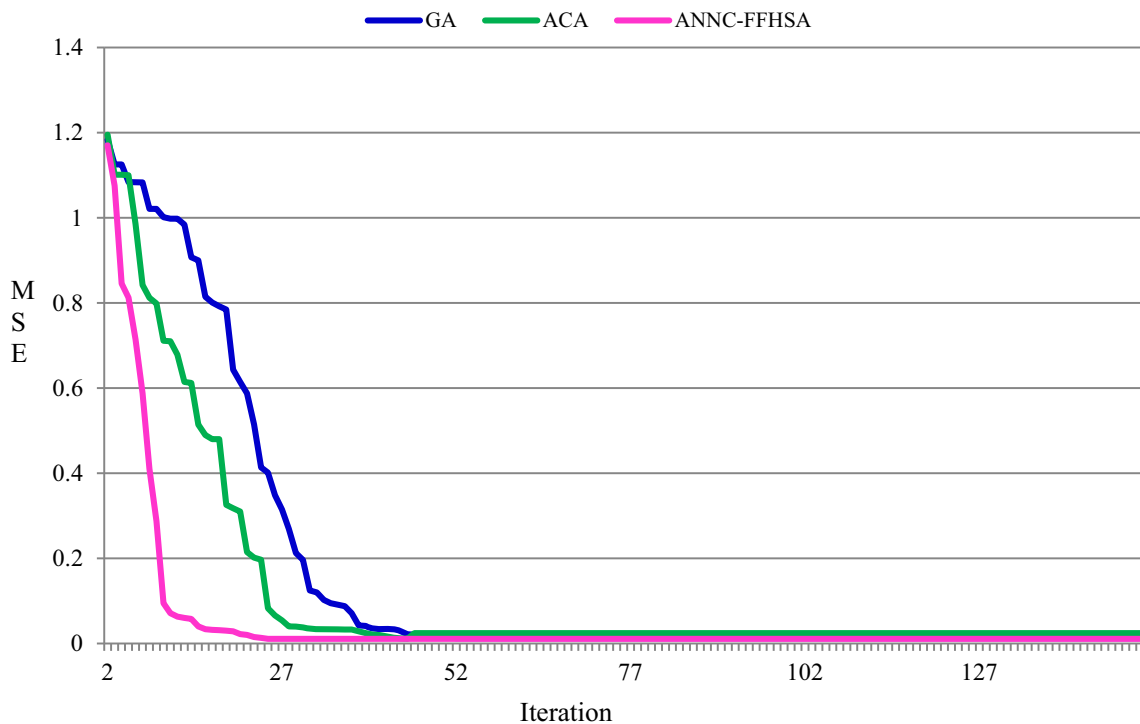
Fig. 12 Comparison of convergence characteristics for case-1

method that was developed effectively mitigated the distortions in the source current. As a result, the THD of the current decreased significantly, dropping from 29.94 to 3.61%. Additionally, the PF increased substantially to 0.99899, which is very close to unity. In addition, the proposed technique regulates the DLCV by maintaining the constant voltage of 700 V

as highlighted in Fig. 13c for constant 1000W/m^2 irradiation and 25^{0}c of constant temperature.

In Case 2, much like in Case 1, balanced V_S is employed. To assess the effectiveness of SAPF, a 30% voltage swell was induced in the time interval from 0.4 s to 0.5 s. However, ANNC identifies the hike in voltage in the grid current and eliminates it by injecting the required compensating voltage
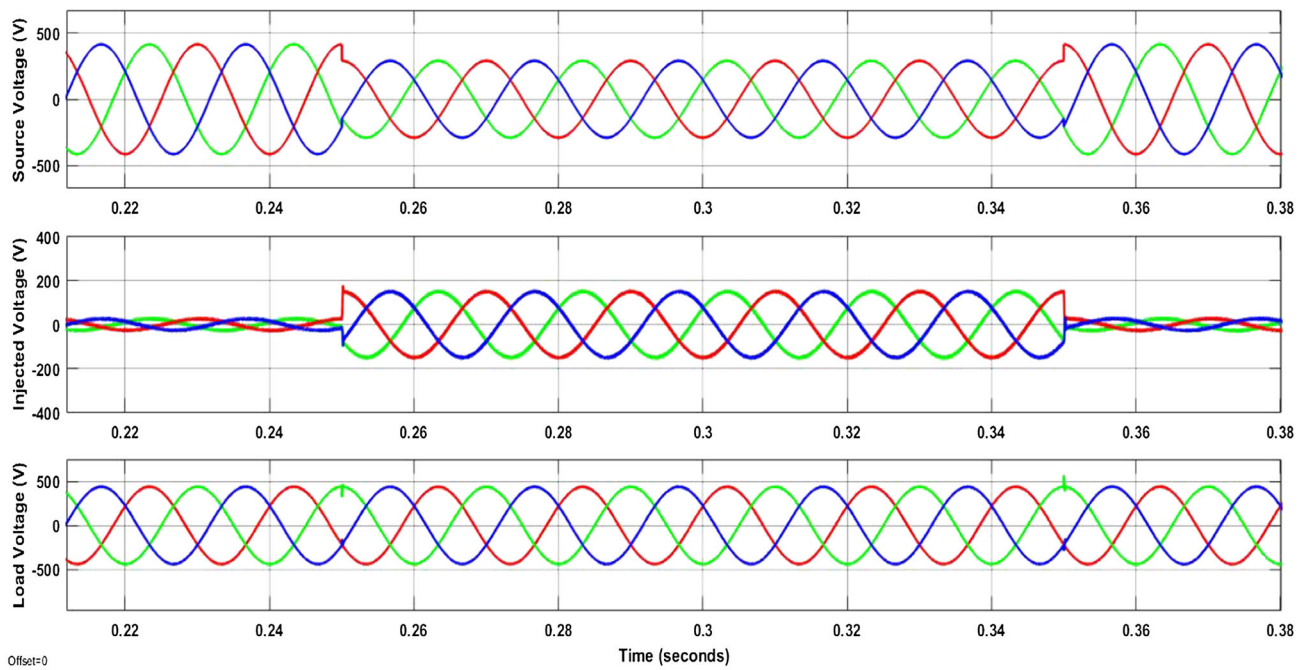
(a) Supply voltage with sag, seires compensated voltage, Load terminal voltage
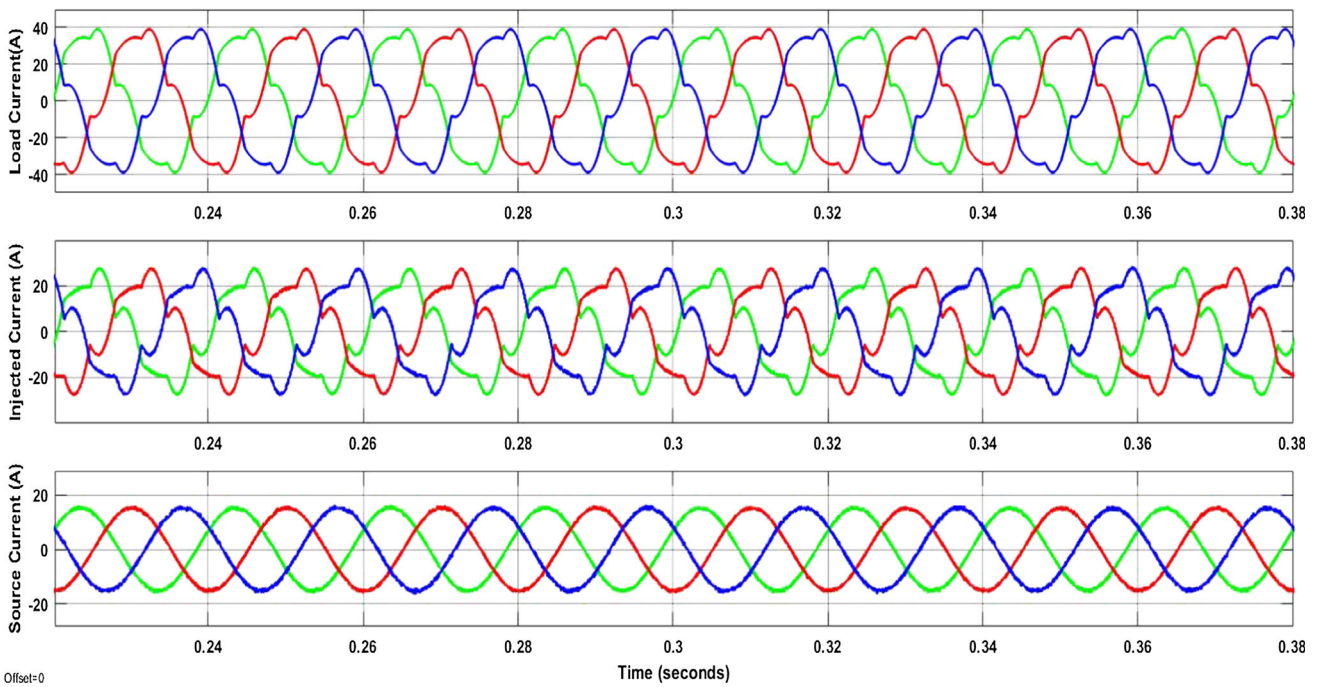
(b) Load terminal current, shunt compensated current, source voltage

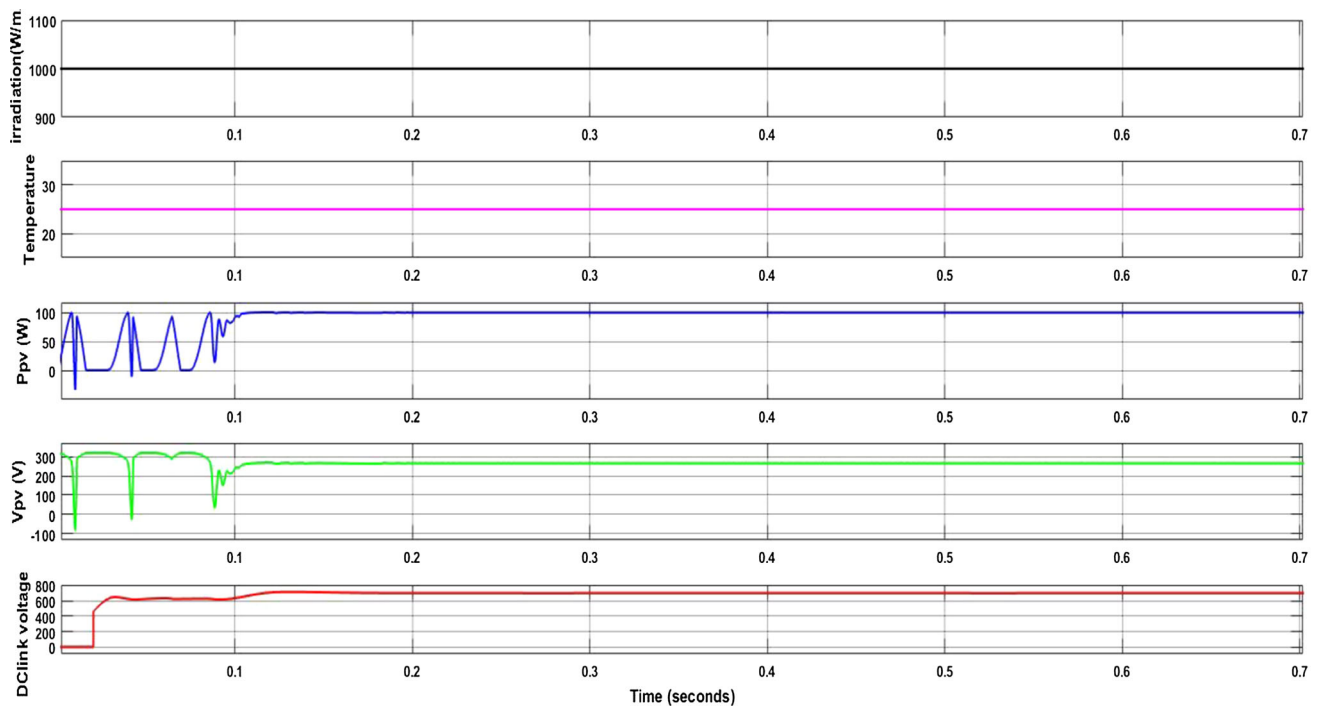**Fig. 13** Signal for the suggested method for the case study one

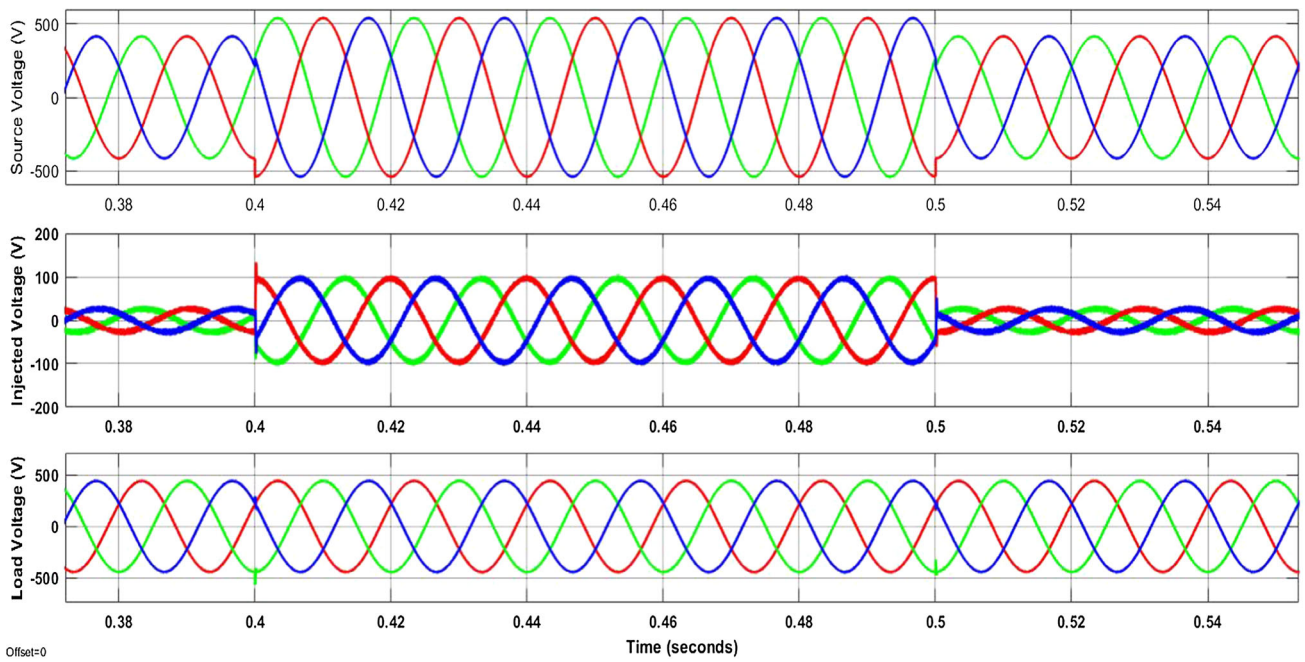(c) G, Temperature, P_{PV}, V_{PV}, V_{dc}

Fig. 13 continued

as illustrated in Fig. 14a. The i_l waveform was identified to be sinusoidal and unbalanced due to the combination of load 2 & 3. To demonstrate the variation in load current waveform load 3 is included at 0.6 s as seen in Fig. 14b. However, the suggested method successfully suppresses current THD, i.e. from 11.54% to 3.58%, which is lesser than other techniques and the PF rises to almost unity. Here, variable G and load change is considered simultaneously under constant temperature of 25 °C. However, the suggested method maintains constant DLCV of 700 V during G variations as shown in Fig. 14c.

In case3, the V_S is selected to be balanced and validated by inserting a disturbance from 0.6 to 0.7 s as demonstrated in Fig. 15a. Nonetheless, the ANNC successfully identifies and mitigates the disturbance by delivering the necessary voltage, as demonstrated in Fig. 13a. Likewise, to assess the effectiveness of the SHAPF, Load 1, in combination with Load 3, was taken into account. This combination resulted in a highly polluted and unbalanced current waveform, as depicted in Fig. 15b. The proposed approach effectively eliminates the imperfections and corrects the imbalance in the current signal. The THD of current signal falls from 24.33 to

3.48%, and the PF rises to almost unity. Besides, the proposed controller keeps DLCV constant for temperature variation as shown in Fig. 15c.

For Case 4, unbalanced V_S is selected. The ANNC-controlled SAPF successfully detects these imbalances and efficiently rectifies them, as depicted in Fig. 16a. In this scenario, Load 1 was connected in combination with Load 2 and Load 3. Load 2 was introduced at 0.3 s, and Load 3 at 0.5 s, resulting in a polluted and unbalanced load current waveform, as illustrated in Fig. 16b. The THD of the current was notably reduced, dropping from 21.86 to 4.51%, and the PF increased to unity. In addition, the proposed controller holds constant DLCV during load variation, temperature as well as irradiation variation successfully shown in Fig. 16c.

Table 6 gives the THD and PF comparison of the proposed method (ANN-FFHSA) with those of other standard methods like GA, PS-O and other controllers available in the survey. It clearly exhibits that proposed method has much lower THD and higher PF when compared to other techniques. Figure 12 portrays that proposed FFHSA reaches to lower MSE of 0.01107 in lower number of iterations (25) has fast convergence when compared GA (52) and ACA (45).

(a) Supply voltage with sag, seires compensated voltage, Load terminal voltage
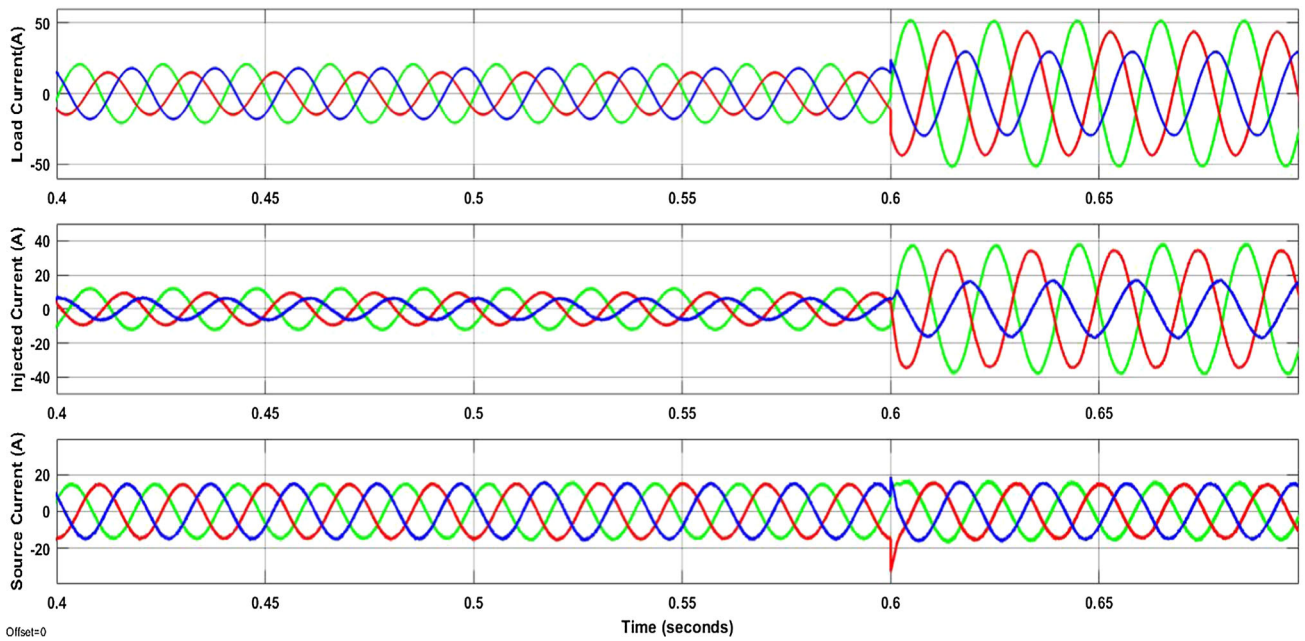
(b) Load terminal current, shunt compensated current, source voltage

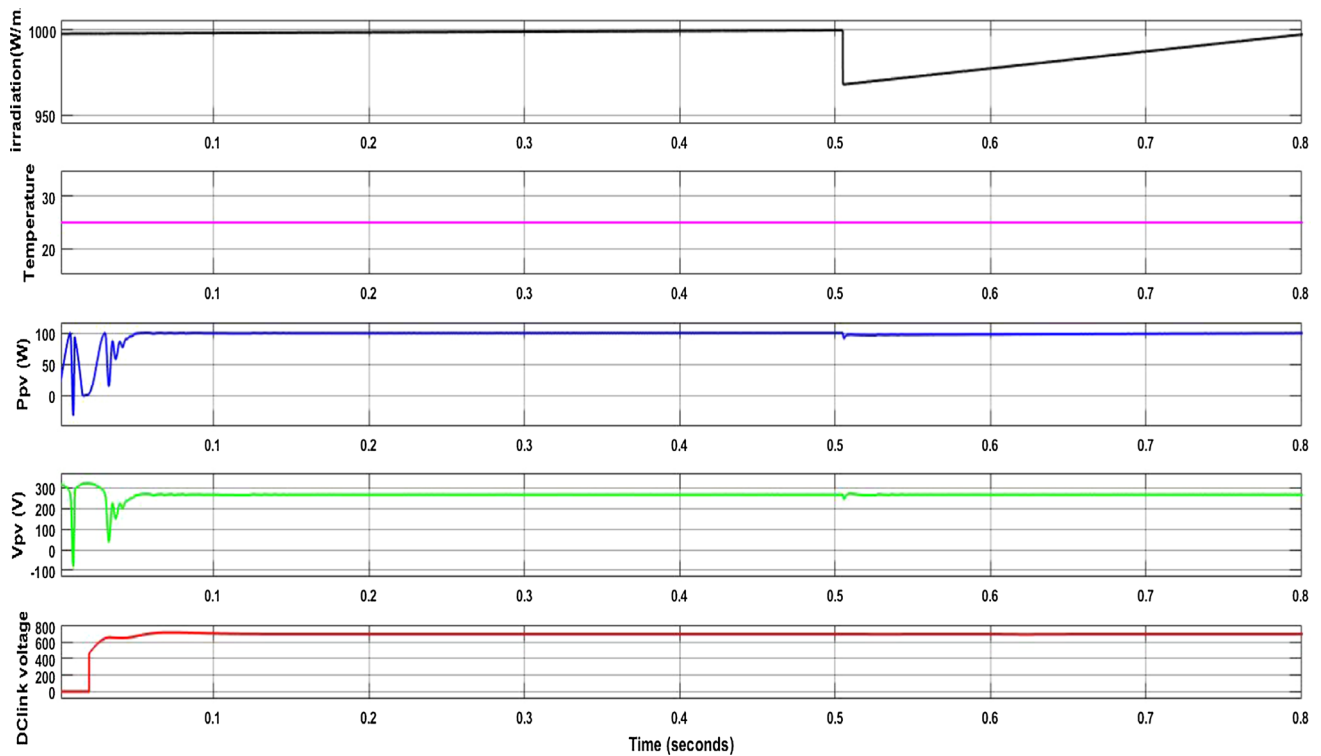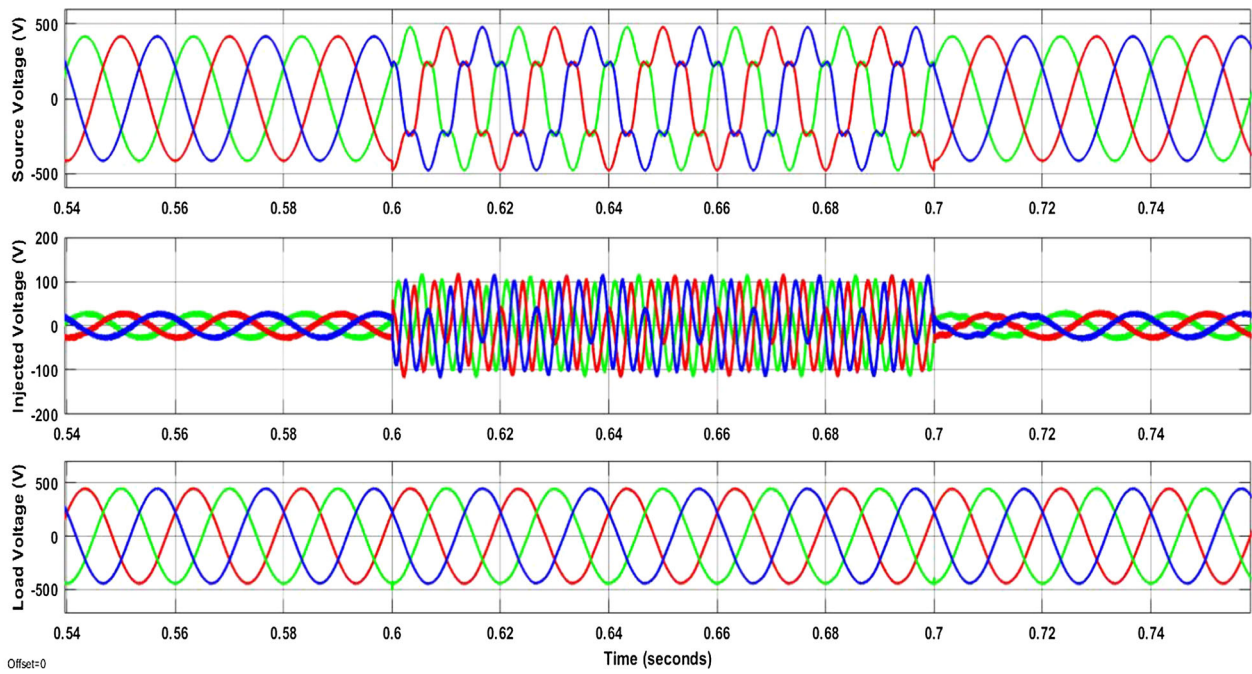**Fig. 14** Signal for the suggested method for the case study two

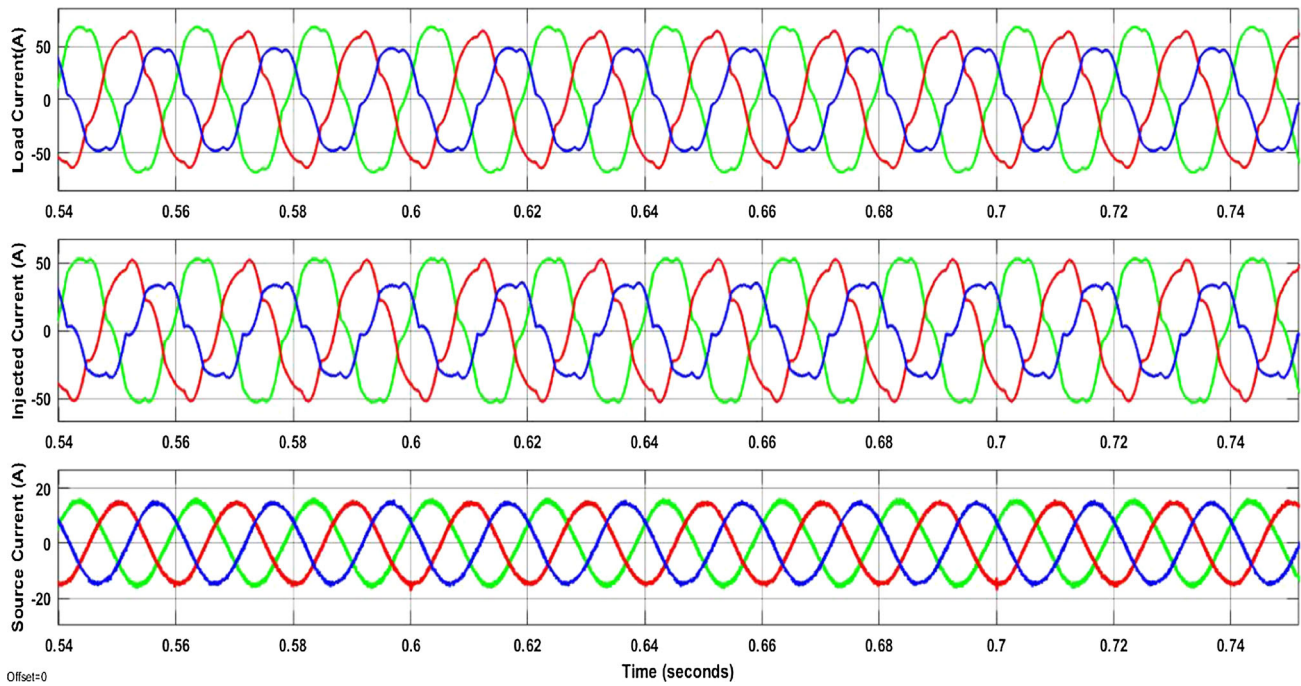(c) G, temperature, P_{PV}, V_{PV}, V_{dc}

Fig. 14 continued

The optimized MSE values of proposed method with GA, ACA are listed in Table 7. In Table 8, we compare the maximum, minimum, and average of THD values achieved by the 50 trials for case-1 using the PPFO method. Additionally, the success rate is also provided within the table. It reveals that the average THD attained by the FFHSA algorithm is much close to the lowest THD value. Moreover, compared to current methods, the success rate after 50 trials is higher. These results, which show both a higher success rate and lower THD, provide statistical evidence of the robustness of

the proposed method in its ability to consistently converge towards the best global solution. However, Fig. 17 represents the spectrum of source current for the proposed system for all the test cases. The switching frequencies [24] and sampling time are 10 kHz and 10 μs. Furthermore, Fig. 18 shows the superior performance of the proposed approach in rapidly achieving stability in DLCV, taking less than 0.1 s, which is notably shorter than the durations required by alternative methods.
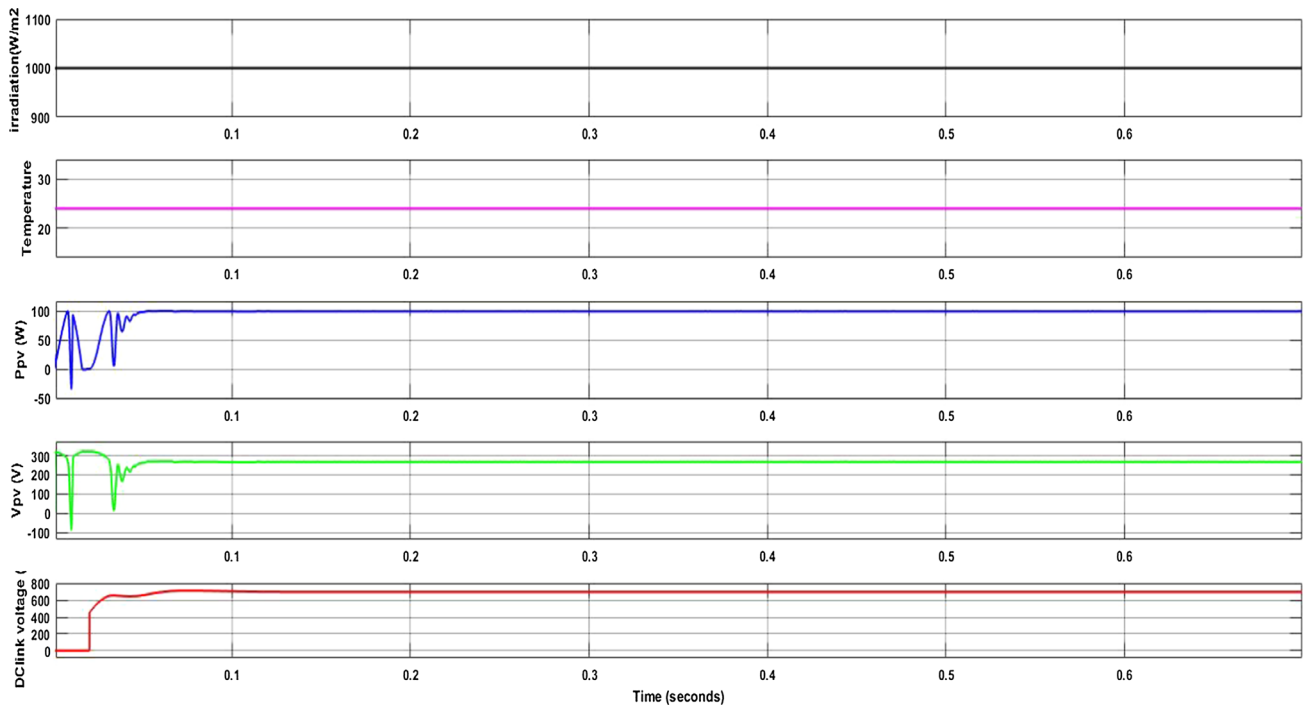
(a) Supply voltage with sag, seires compensated voltage, Load terminal voltage
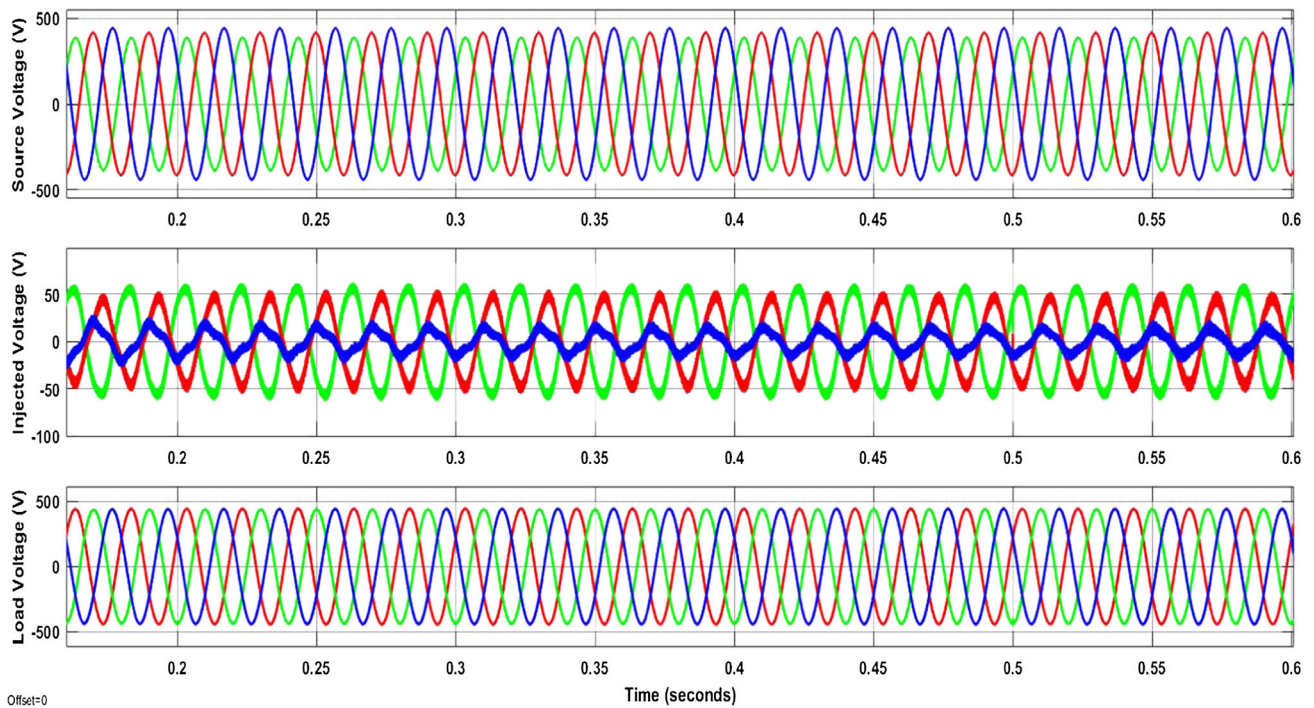

(b) Load terminal current, shunt compensated current, source voltage

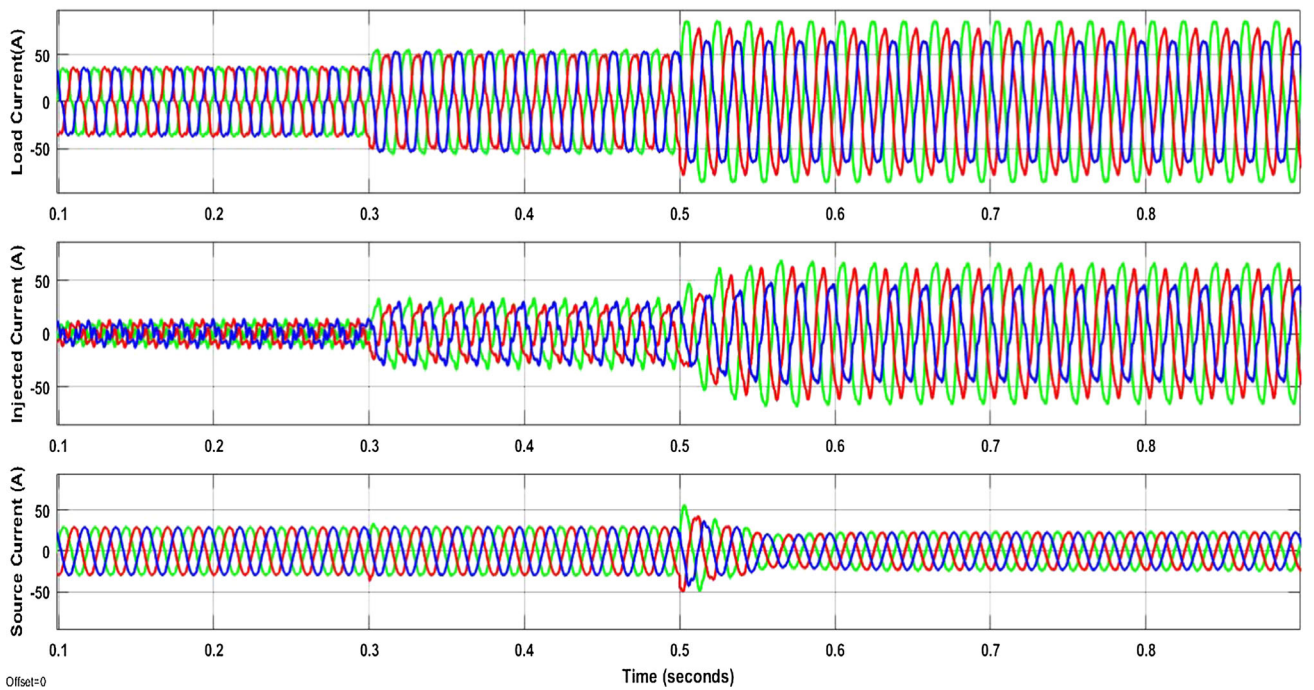**Fig. 15** Signal for the suggested method for the case study three

(c) G, temperature, P$_{PV}$, V$_{PV}$, V_{dc}
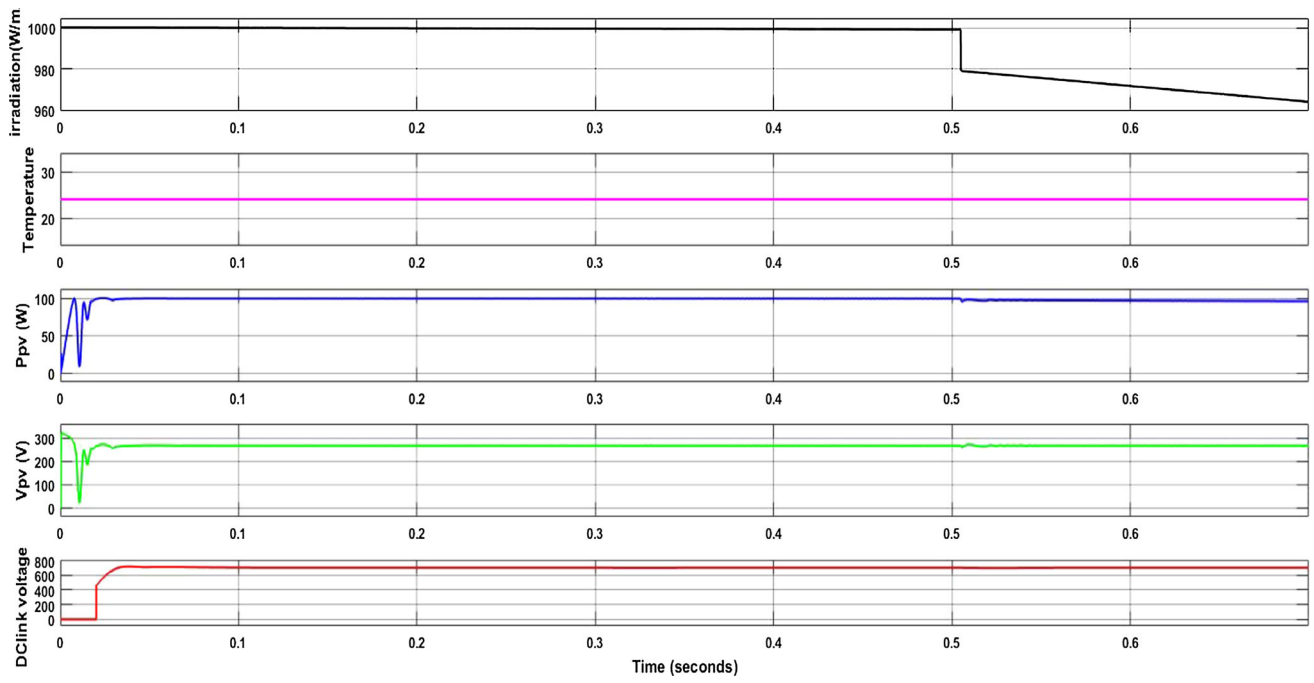
Fig. 15 continued

(a) Supply voltage with sag, seires compensated voltage, Load terminal voltage

(b) Load terminal current, shunt compensated current, source voltage

Fig. 16 Signal for the suggested method for the case study four

(c) G ,temperature, P$_{PV}$, V$_{PV}$, V_{dc}

Fig. 16 continued

Table 6 THD and PF comparison

Case	Method	THD	PF		
			Phase-a	Phase-b	Phase-c
1	NO UPQC	29.94	0.7674	0.7775	0.7952
	FFHSA	**3.61**	**0.9989**	**0.9899**	**1**
	GA	4.07	0.9787	0.9768	0.9209
	ACA	3.94	0.9998	0.9925	0.9974
	p-q	4.02	0.9524	0.9554	0.9586
	SRF	3.98	0.9657	0.9756	0.9778
	SRF [28]	5.47	–	–	–
2	NO UPQC	11.54	0.8814	0.8972	0.8301
	FFHSA	**3.48**	**1**	**1**	**0.9999**
	GA	4.98	1	0.9984	0.9978
	ACA	4.74	0.9999	0.9889	0.9945
	p-q	4.72	0.9862	0.9879	0.9865
	SRF	4.27	0.9878	0.9875	0.9867
3	NO UPQC	24.33	0.8115	0.8908	0.8017
	FFHSA	**3.48**	**1**	**0.9999**	**1**
	GA	3.79	0.9968	0.9849	0.9889
	ACA	3.69	0.9908	0.9817	0.9827
	p-q	3.78	0.9973	0.9987	0.9978
	SRF	3.57	0.9978	0.9989	0.9979
4	NO UPQC	21.86	0.7352	0.7496	0.7991
	FFHSA	**4.51**	**0.9999**	**1**	**0.9997**
	GA	4.18	0.9324	0.9651	0.9878
	ACA	3.43	0.9881	0.9857	0.9858
	p-q	3.92	0.9978	0.9984	0.9988
	SRF	3.47	0.9989	0.9997	0.9994

Bold values indicate the results of proposed method to exhibit its superiority to the compared methods

Table 7 Comparison of MSE

| Case	Method	MSE
1	GA	0.01254
	ACA	0.01129
	ANNC-FFHSA	**0.01107**
2	GA	0.02728
	ACA	0.02704
	ANNC-FFHSA	**0.02041**
3	GA	0.01925
	ACA	0.01472
	ANNC-FFHSA	**0.01201**
4	GA	0.07814
	ACA	0.07451
	ANNC-FFHSA	**0.05148**

Bold values indicate the results of proposed method to exhibit its superiority to the compared methods
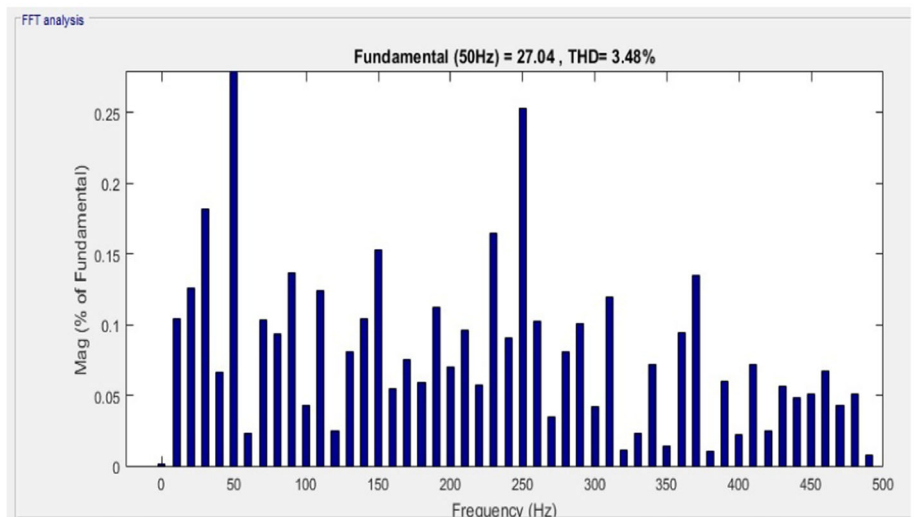
Table 8 Statistical comparison of THD result for case-1

Optimization method	THD			% Success rate
	Maximum value	Minimum value	Average	
GA	5.61	4.07	4.84	77
ACA	4.27	3.94	4.10	84
FFHSA	3.59	3.61	3.60	90

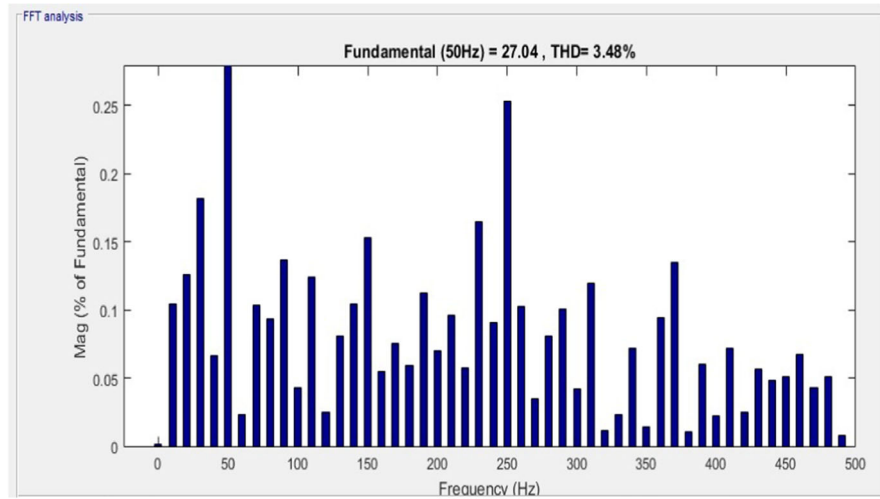**Fig. 17** THD spectrum for all case studies
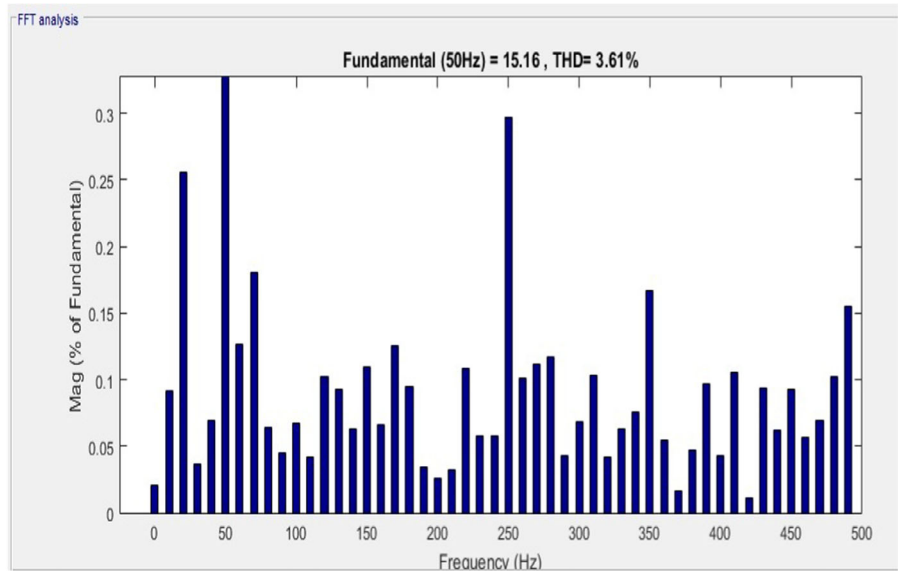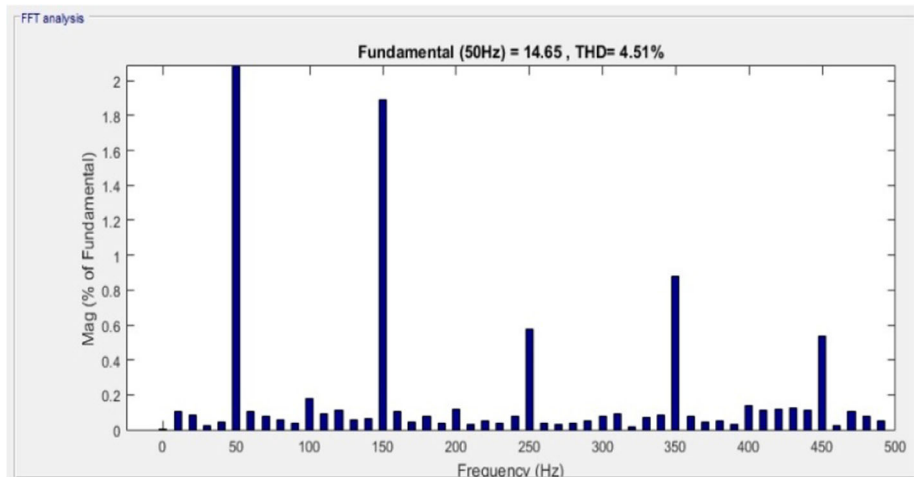

(a) Case-1

(b) Case-2

Fig. 17 continued
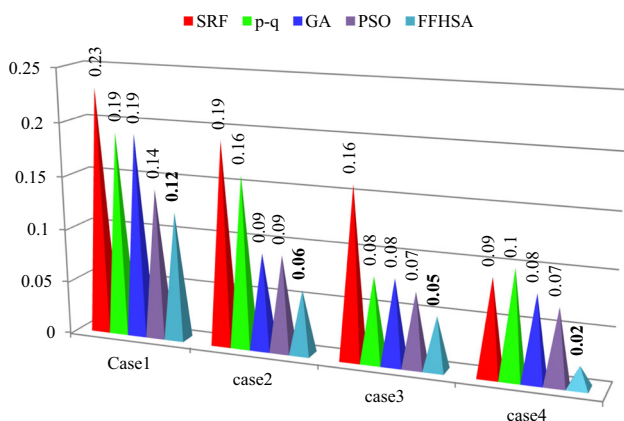

(c) Case-3

(d) Case-4

Fig. 18 Comparison plot of time (sec) taken to reach DLCV stable

5 Conclusion

This work suggests a AI approach for a solar battery-connected UPQC utilizing an ANNC. The ANNC, trained using the LMBP algorithm, is recommended for the integration of solar batteries with the UPQC. The objective is to generate the necessary reference signals for the shunt and series VSCs without the need for conventional transformations such as abc to dq0 to αβ. In addition, the ANFIS parameters are optimally selected by adopting FFHSA algorithm with a view of minimizing MSE effectively. However, the proposed UPVBSS maintains constant DLCV during loads and solar irradiation, temperature variations, suppress the current harmonics improves the shape of current wave-

form thereby boosting up the PF, eliminates the fluctuations of voltage. After analyzing the THD and PF of the system in the absence of the UPQC, the THD values were found to be 29.94% for case1, 11.54% for case2, and 24.33% and 21.86% for case3 and 4, respectively. However, through the implementation of the proposed FFHSA, the THD values were significantly reduced to 3.61%, 3.48%, 3.48%, and 4.51% for the respective cases. This clearly demonstrates that the FFHSA method effectively brought down the THD to acceptable levels and improved the PF to nearly unity. In future, the developed method can be expanded for the microgrid associated multilevel UPQC. In addition, the controllers and parameters can be optimally tuned by using advanced metaheuristic algorithms.

Author contributions Data curation was done by KOS, GSR, KAS, SRI, KK and PKB; formal analysis was done by KOS and IC; funding acquisition was done by IC and PKB; methodology was done by KOS and GSR; project administration was done by PKB; resources were done by SRI and KK; supervision was done by PKB and KAS; and writing–original draft were done by KOS, SRI PKB. All authors have read and agreed to the published version of the manuscript.

Declarations

Competing interests The authors declare no competing interests.

References

1. Yang D, Ma Z, Gao X, Ma Z, Cui E (2019) Control strategy of intergrated photovoltaic-UPQC system for DC-bus voltage stability and voltage sags compensation. Energies 12:4009. https://doi.org/10.3390/en12204009
2. Nkado F, Nkado F, Oladeji I, Zamora R (2021) Optimal design and performance analysis of solar PV integrated UPQC for distribution network. Eur J Electr Eng Comput Sci 5(5):39–46
3. Vinnakoti S (2018) ANN based control scheme for a three-level converter based unified power quality conditioner. J Electr Syst Inf Technol 5(3):526–541
4. Mahar H, Munir HM, Soomro JB, Akhtar F, Hussain R, Elnaggar MF, Guerrero JM (2022) Implementation of ANN controller based UPQC integrated with microgrid. Mathematics 10(12):1989
5. Nagireddy VV, Kota VR, Kumar DA (2018) Hybrid fuzzy backpropagation control scheme for multilevel unified power quality conditioner. Ain Shams Eng J 9(4):2709–2724
6. Hoon Y, Mohd Radzi MA, Hassan MK, Mailah NF (2017) Control algorithms of shunt active power filter for harmonics mitigation: a review. Energies 10(12):2038
7. Cholamuthu P, Irusappan B et al (2022) A grid-connected solar PV/wind turbine based hybrid energy system using ANFIS controller for hybrid series active power filter to improve the power quality. Int Transact Electr Energ Syst 9374638:14
8. Lei T, Riaz S, Zanib N, Batool M, Pan F, Zhang S (2022) Performance analysis of grid-connected distributed generation system Integrating a hybrid wind-PV farm using UPQC. Complexity 4572145:144
9. Okwako OE, Lin Z-H, Xin M, Premkumar K, Rodgers AJ (2022) Neural network controlled solar PV battery powered unified power quality conditioner for grid connected operation. Energies 15:6825. https://doi.org/10.3390/en15186825
10. Mishra AK, Das SR, Ray PK, Mallick RK, Mohanty A, Mishra DK (2020) PSO-GWO optimized fractional order PID based hybrid shunt active power filter for power quality improvements. IEEE Access 8:74497–74512
11. Chandrasekaran K, Selvaraj J, Amaladoss CR, Veerapan L (2021) Hybrid renewable energy based smart grid system for reactive power management and voltage profile enhancement using artificial neural network. Energy Sourc Part A Recov Util Environ Eff 43(19):2419–2442. https://doi.org/10.1080/15567036.2021.1902430
12. Srilakshmi K, Krishna Jyothi K, Kalyani G, Sai Prakash Goud Y (2023) Design of UPQC with solar PV and battery storage systems for power quality improvement. Cybern Syst Int J. https://doi.org/10.1080/019697222175144
13. Sarker K, Chatterjee D, Goswami SK (2021) A modified PV-wind-PEMFCS-based hybrid UPQC system with combined DVR/STATCOM operation by harmonic compensation. Int J Modell Simul 41(4):243–255
14. Hoon Y, Radzi MAM et al (2019) Shunt active power filter: a review on phase synchronization control techniques. Electronics 8:791. https://doi.org/10.3390/electronics8070791
15. Nicola M, Nicola CI, Sacerdoţianu D, Vintilǎ A (2023) Comparative performance of UPQC control system based on PI-GWO, fractional order controllers, and reinforcement learning agent. Electronics 12(3):494. https://doi.org/10.3390/electronics12030494
16. Sayed JA, Sabha RA, Ranjan KJ (2021) Biogeography based optimization strategy for UPQC PI tuning on full order adaptive observer based control. IET Gener Transm Distrib 15:279–293
17. Renduchintala UK, Pang C, Tatikonda KM, Yang L (2021) ANFIS-fuzzy logic based UPQC in interconnected microgrid distribution systems: modeling, simulation and implementation. J Eng 2021(1):6–18. https://doi.org/10.1049/tje2.12005
18. Rajesh P, Shajin FH, Umasankar L (2021) A novel control scheme for PV/WT/FC/battery to power quality enhancement in micro grid system: a hybrid technique. Energ Sourc Part A Recov Util Environ Eff 1–18.
19. Pazhanimuthu C, Ramesh S (2018) Grid integration of renewable energy sources (RES) for power quality improvement using adaptive fuzzy logic controller based series hybrid active power filter (SHAPF). J Intell Fuzzy Syst 35:749–766
20. Srilakshmi K, Sujatha CN, Balachandran PK, Mihet-Popa L, Kumar NU (2022) Optimal design of an artificial intelligence controller for solar-battery integrated UPQC in three phase distribution networks. Sustainability 14(21):13992
21. Kenjrawy H, Makdisie C, Houssamo I, Mohammed N (2022) New modulation technique in smart grid interfaced multilevel UPQC-PV controlled via fuzzy logic controller. Electronics 11:919. https://doi.org/10.3390/electronics11060919
22. Srilakshmi K, Srinivas N et al (2022) Design of soccer league optimization based hybrid controller for solar-battery integrated UPQC. IEEE Access 10:107116–107136. https://doi.org/10.1109/ACCESS.2022.3211504
23. Vinnakoti S, Kota VR (2017) Implementation of artificial neural network based controller for a five-level converter based UPQC. Alex Eng J Elsevier 57(3):1475–1488. https://doi.org/10.1016/j.aej.2017.03.027
24. Mansor MA, Hasan K, Othman MM, Noor SZBM, Musirin I (2020) Construction and performance investigation of three-phase solar PV and battery energy storage system integrated UPQC. IEEE Access 8:103511–103538. https://doi.org/10.1109/ACCESS.2020.2997056
25. Das SR, Mishra AK, Ray PK, Salkuti SR, Kim SC (2022) Application of artificial intelligent techniques for power quality improvement in hybrid microgrid system. Electronics 11(22):3826. https://doi.org/10.3390/electronics11223826

26. Das SR, Ray PK, Mishra AK, Mohanty A (2021) Performance of PV integrated multilevel inverter for PQ enhancement. Int J Electron 108(6):945–982. https://doi.org/10.1080/00207217.2020.1818848

27. Ranjan Das S, Mishra AK, Ray PK, Mohanty A, Mishra DK, Li L, Mallick RK (2020) Advanced wavelet transform based shunt hybrid active filter in PV integrated power distribution system for power quality enhancement. IET Energ Syst Integr 2(4):331–343. https://doi.org/10.1049/iet-esi.2020.0015

28. Mishra AK, Nanda PK, Ray PK et al (2023) IFGO optimized self-adaptive fuzzy-PID controlled HSAPF for PQ enhancement. Int J Fuzzy Syst 25:468–484. https://doi.org/10.1007/s40815-022-01382-0

29. Mishra AK, Nanda PK, Ray PK et al (2023) DT-CWT and type-2 fuzzy-HSAPF for harmonic compensation in distribution system. Soft Comput. https://doi.org/10.1007/s00500-023-08286-7